Chapter 3 Results and Discussions

3-1 Structure Evolution and initial growth of Ni ultrathin Films on Pt(111)

Recently, Ni-Pt-based thin films and alloys have attracted considerable interest due to their magnetism and catalytic activity. Ni-Pt alloys have been used as catalysts in many technologically important fields including petroleum refining and automotive emission control.[41] The Ni ultrathin films on Pt(111) substrate has a tendency of large perpendicular magnetic anisotropy (PMA) at low temperature.[42,43] Adding Ni atoms on Co-Pt thin films or multilayers can decrease the Curie temperature and have some interesting changes in magnetic properties.[44-47] Recently, Wilhelm *et al.* found that the hybridization effects between Ni and Pt are mostly localized at the interface and result in a reduction of Ni moment and spin polarization of Pt.[48] The study of growth behavior and alloy formation of Ni films on Pt can be beneficial to understand these magnetic properties and catalytic activities.

In this section, low-energy electron diffraction (LEED) and Auger electron spectroscopy (AES) were used to study the initial growth of Ni ultrathin films deposited on a Pt(111) surface. Some interesting structural phases were observed. The alloy formation at different coverage was investigated.

AES was used to study the growth mode when Ni ultrathin films were grown on Pt(111) at room temperature. Auger signals of Pt NNV 237 eV, Ni LVV 848 eV and Ni MVV 102 eV as a function of the deposition time are shown in Fig. 3-1a. These Auger intensities increase linearly between 0 and 800 s, with the exception of a kink located at 400 s. These curves then change to an exponential tendency after t > 800 s. The change of the slope on the Auger uptake curve is interpreted as the layer-by-layer growth of a complete atomic layer on a flat surface.[49,50] The result of Fig. 3-1a indicates that Ni atoms grow 1 ML at about 400 s, and 2 ML at about 800 s, in the layer-by-layer growth and then develop into three-dimensional island growth.

The oscillation of LEED intensity has been used to measure the number of layers of a MBE growth.[50,51] The peak height intensity of LEED (0,0) beam versus deposition time is shown in Fig. 3-1b. The incident electron energy is 73 eV. The out-of-phase condition, $\phi(0,0) = \Delta k_{\perp} h = n\pi$, n: add number, was taken in our experiment, where $\Delta k_{\perp}$ is the momentum transfer perpendicular to the surface, and $h = 2.03$ Å is the step height of the adsorbed Ni atoms. The out-of-phase condition in the diffraction is more sensitive to the surface step density and can oscillate in a layer-by-layer growth.[52] In Fig. 3-1b, the maximum of the intensity means that one monolayer grows completely, so that 1 ML and 2 ML Ni thin films occur at 400 s and

800 s, respectively. The result of LEED is consistent with that of AES. From the results of AES and LEED, we can conclude that the growth of Ni/Pt(111) is the Stranski-Krastanov mode. It grows 2 ML in a layer-by-layer mode, and then turns into 3-D island growth. This conclusion is agreed with the result of X-ray photoelectron diffraction.[53]

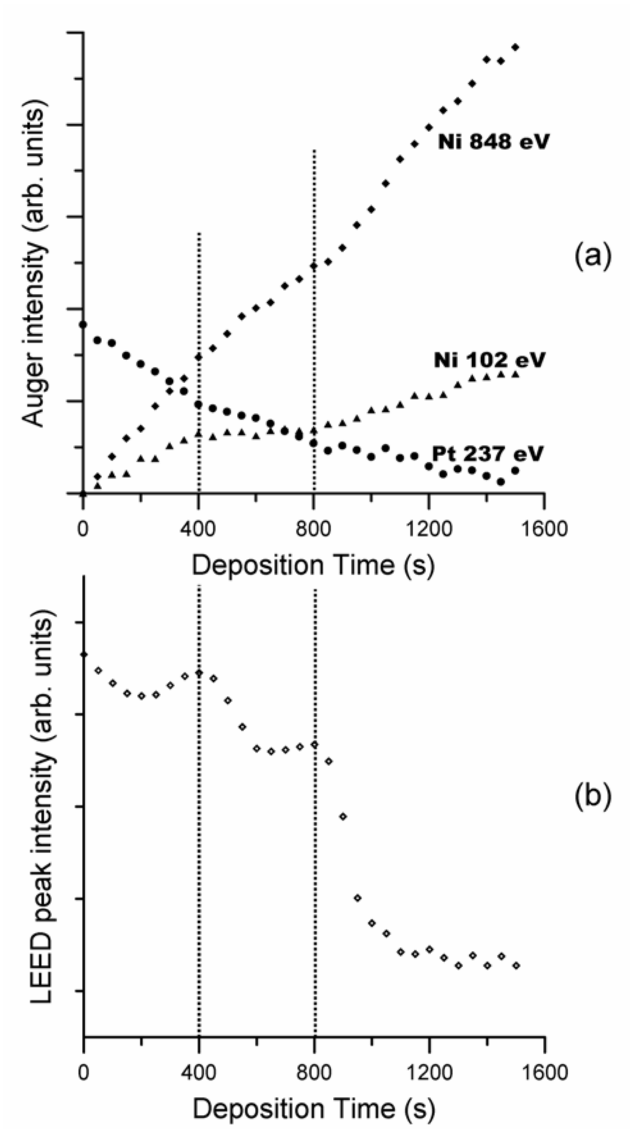

Fig. 3-1 (a) Auger uptake curves for Ni LVV 848 eV, Ni MVV 102 eV and Pt NNV 237 eV Auger peak intensity versus deposition time. The break points at t = 400 and 800 seconds correspond to 1.0 ML and 2.0 ML of Ni coverage. (b) The intensity of the specular beam of LEED as a function of deposition time (I-t profile). The beam energy of 73 eV was used. Two peaks locate at the same deposition times that of AES break points.

The structural evolution of Ni/Pt(111) at different coverage was observed by LEED. The LEED pictures and corresponding schematic patterns are shown in Fig.

3-2. When the coverage of Ni is below 0.2 ML, the (1×1) LEED spots are observed as shown in Fig. 3-2a. This is a pseudo-(1×1) structure because the LEED spots are slightly diffused if compared to the clean Pt(111) LEED pattern. According to the LEED I-V profile by Atrei *et al.*, Ni atoms prefer to occupy the 3-fold hollow sites with fcc stacking sequence initially.[54] This is consistent with our observation. The LEED pattern in Fig. 3-2a also shows the 3-fold symmetry. When the coverage is between 0.3 ML to 0.9 ML, the LEED pattern changes to the $(\sqrt{3} \times \sqrt{3})\mathrm{R}\,30^\circ$ as shown in Fig. 3-2b. The $(\sqrt{3} \times \sqrt{3})\mathrm{R}\,30^\circ$ is a well known structure for a metal adsorbate on Pt(111) surface, for example Ag/Pt(111),[55] and K/Pt(111).[56] A very interesting new phase was observed when the thickness of Ni is between 1.0 ML and 1.2 ML as shown in Fig. 3-2c. An extra LEED spot appears on each diagonal line outside the original spot of Pt(1×1) LEED pattern. This structure means that Ni atoms epitaxially grow with respect to the Pt substrate, but having a different lattice constant. The nearest neighboring distance of Pt and Ni atoms is 2.77 Å and 2.49 Å, respectively. The ratio of reciprocal lattice constant is about $\frac{1}{1.11}\,(\approx 0.9)$. It is consistent with the ratio of the distances between Pt, Ni LEED spots and the specular beam. A Ni(1×1) structure accompanying some satellites LEED pattern was observed for the coverage from 1.3 ML to 6 ML as shown in Fig. 3-2d. The intensity of these fine diffraction satellites becomes blurred as the Ni thin film becomes too thick. This incommensurate LEED structure indicates an incoherent epitaxy of Ni overlayers on Pt(111). Similar fine structure of LEED satellites have been observed in thin film systems with large lattice mismatch, such as Co/Pt(111),[57] Pt/Ni(111)[58] and Cu/Ru(0001).[59] The clearest satellite LEED pattern occurs in the Ni coverages between 1.3 and 2.0 ML. The intensities of the inner satellite spots on each diagonal line become stronger than the other ones after the coverages are larger than 2.6 ML, but these fine direction satellites become gradually blurred as the coverage of Ni thin films is too thick. The LEED pattern was monitored for every 0.4 ML. However, the satellite LEED pattern did not change for the coverages from 1.3 to 6 ML. The LEED patterns due to rotated domains or corrugated structure of strained Cu layers on Ru(0001) were not observed in our system.[59] This incoherent epitaxial growth may cause the intensity of the LEED specular beam to decay rapidly as shown in Fig. 3-1b.

When the coverage further increases, the fine spots of the satellites gradually disappear and an extra spot appears at the center of each side of the triangle as shown in Fig. 3-2e. This is the (2×2) structure and can be observed in the coverage range between 6 ML and 10 ML. The similar LEED pattern has also been found on the surface of an 8 ML thick iron oxide film on Pt(111)[60] and on the surface of 4.5-7 ML cobalt films on Pt(111).[17] These additional spots have been interpreted as a particular

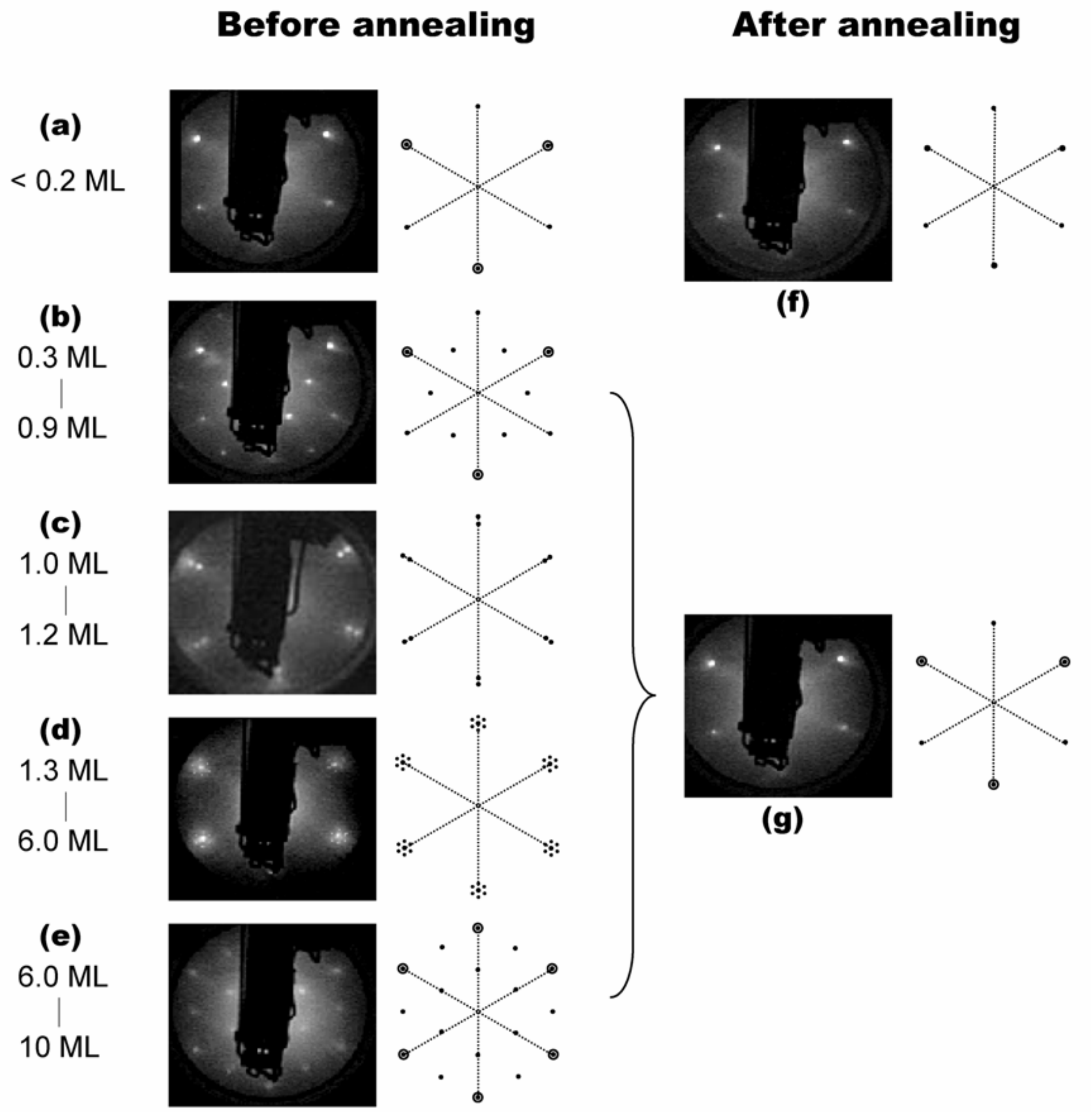

Fig. 3-2 LEED patterns for different coverage observed at room temperature before the annealing ((a) to (e)), and observed at room temperature after annealing ((f) and (g)). In the schematic LEED diagrams, the area of the circle is proportional to the spot size of LEED. Detailed description is given in the text.

arrangement of the step structure at the topmost layer. The step height and the step orientation can be determined by analyzing the data of the I-V profile for each diffraction beam of the (2×2) LEED pattern.[60]

All the above LEED patterns were observed at room temperature. The LEED patterns change to the (1×1) structure as shown in Fig. 3-2f and 3-2g after the ultrathin films have been annealed at 750 K for 5 minutes and observed at room temperature. The (1×1) LEED spots of Fig. 3-2f are sharper than that of Fig. 3-2a. The sharp (1×1) pattern is due to the surface alloy lattice formed upon diffusion of Ni adatoms toward the bulk as a consequence of the annealing treatment. This phenomenon will be discussed later. The (1×1) LEED pattern after annealing becomes blurred and the spot size increases as shown in Fig. 3-2g when the Ni films become thicker.

The phase diagram of Ni/Pt(111) is summarized in Fig. 3-3. It can be divided into six regions. In region I, the coverage $\Theta < 0.2$ ML, it shows the pseudo-Pt(1×1) structure. The Ni atoms accumulate on Pt(111) with a reciprocal lattice vector of $a^*_{Ni} = a^*_{Pt}$. The adatoms in the overlayer relax to fit the Pt(111) lattice points. In region II, 0.3 ML $\leq \Theta \leq$ 0.9 ML, a $(\sqrt{3}\times\sqrt{3})\mathrm{R}30°$ superstructure of Ni atoms is adsorbed in an ordered state on Pt(111) surface. This structure persists until the annealing temperature reaches 450 K. In region III, 1.0 ML $\leq \Theta \leq$ 1.2 ML, there is the coherent (1×1) structure. Each site on Pt(111) surface is occupied by one Ni atom. Since the lattice constant of Ni is smaller than that of Pt, the coherent structure is reasonable. This structure remains unchanged during the annealing up to a temperature at 475 K. In region IV, 1.3 ML $\leq \Theta \leq$ 6.0 ML, Ni atoms grow by incoherent epitaxy. The fine satellites around the hexagonal Ni(1×1) main spots were observed. In region V, 6.0 ML $\leq \Theta \leq$ 10 ML, additional (2×2) spots appear because of surface steps formed at the topmost layer. After high temperature annealing, LEED pattern shifts to (1×1) structure. All (1×1) LEED patterns in region VI (Θ <10 ML) have the reciprocal vector of Pt. This is the evidence that Ni atoms diffuse into Pt bulk and a disordered Ni-Pt surface alloy formation. Since the Ni-Pt alloy on surface layers is disordered, the background intensity of the (1×1) LEED pattern increases and the LEED spots become blurred.

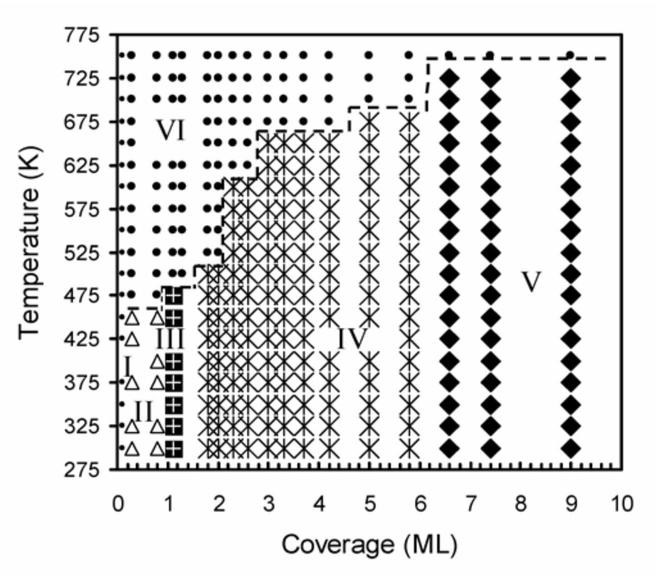

Fig. 3-3 Phase diagram determined by LEED, the structure phase is divided into six distinct regions. The corresponding LEED patterns are shown in Fig. 2. Detailed description is given in this article.

Furthermore, we studied the alloy formation by AES. Ni MVV 102 eV Auger signal was detected. The results are shown in Fig. 3-4. Each experimental value was measured three minutes after the thermal equilibrium reached. All these Auger intensities at different coverage do not change until Ni atoms start to diffuse into Pt bulk. T_a is the temperature value at which the Auger intensity begins to drop, as soon as the Ni-Pt alloy starts to develop. These values of T_a are 450, 475, 500, 600, and 650 K for Ni coverage of 0.8, 1.3, 2.0, 2.3, and 3.0 ML, respectively. T_a rises as the coverage of Ni increases. This behavior is similar to that of Co/Pt(111).[17] This phenomenon may be caused by the adsorbate-adsorbate interaction. This interaction prevents the formation of Ni-Pt alloy. Since the interdiffusion occurs from the Ni-Pt interface, the attraction between Ni atoms needs to be overcome by higher temperature.

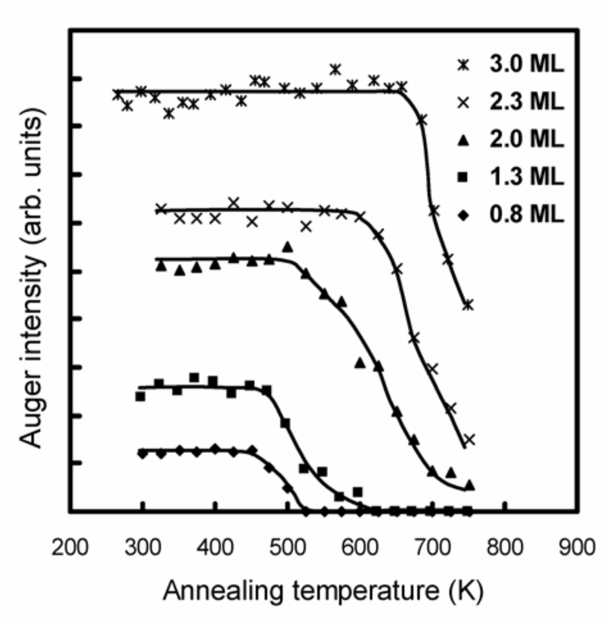

Fig. 3-4 Ni MVV 102 eV Auger peak intensity versus annealing temperature for different Ni coverage on Pt(111) surface. The starting temperature of Ni-Pt alloy formation rises as the coverage of Ni increases.

The dependence of T_a as a function of Ni coverage is shown in Fig. 3-1-5. It is interesting that T_a significantly increases when the coverage is larger than 2 ML. From Fig. 1 we have concluded that the first 2 ML of Ni thin films on Pt(111) are in the layer-by-layer growth and then turns into three dimensional island growth. Fig. 3-1-5 shows that the interdiffusion barrier for the 3-D islands is higher than that for the flat layer in this system.

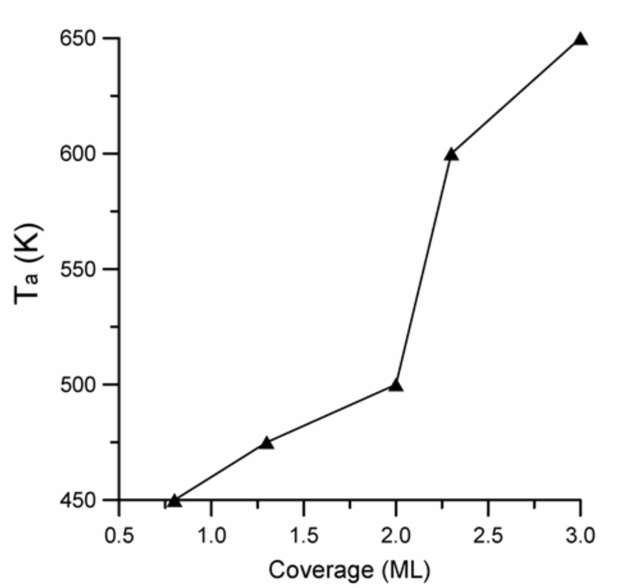

Fig. 3-5 The starting temperature T_a versus Ni coverage. T_a increases significantly after the coverage of Ni is 2 ML during which the growth of Ni turns into 3-D island growth.

The growth of Ni ultrathin films on Pt(111) follows the layer-by-layer growth up to 2 ML, then turns into 3-D island growth. Rich structural phases in this system were observed at different coverage: the pseudo-(1×1) structure for $\Theta<0.2$ ML, the $(\sqrt{3}\times\sqrt{3})R30°$ commensurate superstructure for $0.3\leq\Theta\leq0.9$ ML, the Ni(1×1) spots appearing outside Pt(1×1) LEED spots for $1.0\leq\Theta\leq1.2$ ML, the incoherent epitaxy for $1.3\leq\Theta\leq6.0$ ML, and the (2×2) superstructure for $6.0\leq\Theta\leq10$ ML. The starting temperatures for Ni-Pt alloy formation are 450, 475, 500, 600, and 650 K for Ni coverage of 0.8, 1.3, 2.0, 2.3, and 3.0 ML, respectively.

3-2 Coverage Determination of Ni Ultrathin Films on Pt(111)

Ferromagnetic materials possess unusual magnetic properties in nanoscale solids and have important applications in the microelectronics industry. Therefore, ferromagnetic ultrathin films and multilayers have always attracted the attention of science researchers around the world. Ni-Pt based systems have been used as the catalyst to hasten the reaction of oxidation and hydrogenation.[61,62] In earlier research, Atrei et al. using low-energy electron diffraction intensity analysis observed that the first monolayer of Ni grows pseudomorphically on Pt(111).[63] Sambi et al. demonstrated by using the measurement of X-ray photoelectron diffraction that the Ni ultrathin films exhibit a single domain fcc stacking pseudomorphic with consequent trigonal distortion on Pt(111).[64] Recently a perpendicular magnetic anisotropy was observed in Ni/Pt multilayers.[65,66] However most studies of Pt-Ni based system focused on the investigation of the surface structure and segregation of Pt thin films grown on a single Ni crystal surface.[67-69] We used molecular beam epitaxy to grow Ni ultrathin films on Pt(111). Auger electron spectroscopy (AES) was used to profile the composition in the interfaces, and ultraviolet photoelectron spectroscopy (UPS) was used to investigate the electron structure of the valence band during the thin film growth and the surface alloy formation. The growth mode and structural phases of Ni films on Pt(111) have been reported in our earlier studies.[70] In this paper, with the exception of the comparison between the experimental data and the two theoretical models used for coverage determination, the peak height of the UPS can be used to determine the thickness of ultrathin film. Furthermore, the evolution in electron structure of the valence band was studied in the formation of Ni-Pt alloy.

The coverage determination is an important procedure of a surface study. When the coverage Θ of an adsorbate is less than 1 ML, Θ can be calculated from[71]

$$\frac{I_a}{I_s} = \frac{I_a^\infty}{I_s^\infty} \cdot \frac{\Theta \cdot \left[1 - e^{\frac{-d}{\lambda(E_a)\cos\theta}} \right] \left[\frac{1 + r_s(\varepsilon_a)}{1 + r_a(\varepsilon_a)} \right]}{\left[1 - \Theta + \Theta \cdot e^{\frac{-d}{\lambda(E_s)\cos\theta}} \right]} \tag{3-1}$$

where I_a / I_s is the relative rate of the Auger intensities of the adsorbate and the substrate; I_a^∞ / I_s^∞ is the relative rate of the Auger intensities of the bulk adsorbate and the bulk substrate, which is equivalent to the relative sensitivity of the Auger detector for the adsorbate and substrate; *d* is the atomic size of the adsorbate; $\lambda(E_s)$, $\lambda(E_a)$ are the attenuation lengths or the inelastic mean free paths as a function of the

Auger electron energies E_s and E_a emitted from the substrate and adsorbate, respectively; θ is the angle of the electron emission from the surface normal; $r(\varepsilon_a)$ is the back-scattering term as a function of the core-level energy ε_a of the adsorbate.

When the coverage of the adsorbate is larger than 1 ML, the thickness of the overlayer d' can be calculated by

$$\frac{I_a}{I_s} = \frac{I_a^\infty}{I_s^\infty} \cdot \frac{\left[1 - e^{\frac{-d'}{\lambda(E_a)\cos\theta}}\right]\left[\frac{1 + r_s(\varepsilon_a)}{1 + r_a(\varepsilon_a)}\right]}{e^{\frac{-d'}{\lambda(E_s)\cos\theta}}} \tag{3-2}$$

Eq. (3-2) is obtained by setting $\Theta = 1$ and changing *d* to d' in Eq. (3-1). The atomic size *d* of Ni is 0.222 nm. The values of the back-scattering terms $r_s(\varepsilon_a = 852.7\text{eV})$ for the substrate Pt and $r_a(\varepsilon_a = 852.7\text{eV})$ for the adsorbate Ni are 0.72 and 0.44, respectively, are obtained from the suggested formula of Shimizu *et al.*[71,72] as the listed Eq. 3-3.

$$r = (2.34 - 2.10Z^{0.14})U^{-0.35} + (2.58Z^{0.14} - 2.98) \tag{3-3}$$

where Z is the atomic number, $U = E/E_{AX}$; where E is the energy of the incident electron and E_{AX} is the binding energy from the core level of the excited Auger electron. One must be noticed that the formula above is applied only at the angle to the surface normal of the incident electron beam. Moreover, the Auger electron emission detected in the hemispherical analyzer of our AES system is near the surface normal, and hence $\cos\theta = 1$.

We want to compare our experimental data with the predicted coverage of the adsorbate from Eqs. (3-1) and (3-2). The oscillation of the LEED specular (00) beam intensity has been used to measure the number of layers of a MBE growth.[73] Each maximum of the oscillated LEED (00) beam intensities can be interpreted as the completion of one atomic layer. The LEED (00) beam intensity versus the coverage is shown in Fig. 3-6a. We then measured the corresponding Auger signals of Ni and Pt and calculated the coverage of Ni from Eqs. (3-1) and (3-2).

Two different models provided the formula of the attenuation length from Seah *et al.*[74]

$$\lambda = 538E^{-2} + 0.41(aE)^{0.5} \tag{3-4}$$

where a is the atomic size of the element derived from $a = 10^7\left(\frac{M}{\rho n N_0}\right)^{1/3}$ (in nm), E is the energy of the corresponding Auger electron in eV, and the inelastic mean free path (IMFP) from Tanuma *et al.*[75]

$$\lambda_i = \frac{E}{E_p^{\,2}\left[\beta \ln(\gamma E) - C/E + D/E^2\right]} \tag{3-5}$$

where $E_p = 28.8(\rho N_v/A)^{1/2}$ eV, N_v is the total number of valence electrons per atom or molecular, ρ is in g/cm^3 and A is the atomic or molecular weight. In addition, parameter in the formula is the following:

$$\begin{aligned}
&\beta = -0.10 + \frac{0.944}{(E_p^{\,2} + E_g^{\,2})^{1/2}} + 0.069\rho^{0.1} \\
&\gamma = 0.191\rho^{-0.50} \\
&C = 1.97 - 0.91U \\
&D = 53.4 - 20.8U
\end{aligned} \tag{3-6}$$

where $U = N_v\rho/M = E_p^{\,2}/829.4$, $E_g = 0$ for metal and $N_v = 8$ for Ni. Eqs. (3-4) and (3-5) derived from two different models can be used to determine the attenuation length or the inelastic mean free path λ. The values of $\lambda(E_a = 848eV)$ following Seah's model and Tanuma's model are 1.25 and 1.37 nm respectively, and the values of $\lambda(E_s = 237eV)$ are 0.66 and 0.59 nm, respectively. The ratio of the Auger electron relative sensitivity $I_{Ni}^{\infty}/I_{Pt}^{\infty}$ is 7.82 from the Handbook.[76] Nevertheless, the calculated results after putting these parameters into Eqs. (3-1) and (3-2) do not match well with the experimental results. Recently, a material-to-material dependent correction factor G proposed by Seah *et al* thus introduce in the fomula.[77] The selected correction factors of the elements in this paper are listed in the following Table. 3-1.

TABLE 3-1

Atomic number	Element	Correction factor, G
27	Co	0.75
28	Ni	0.77
47	Ag	0.94
78	Pt	0.86

After multiplication of the correction factor $G_{Ni}/G_{Pt} = 0.90$ on the right-hand side of equations (3-1) and (3-2), the theoretical values are in good agreement with our experimental data as shown in Fig. 3-6b. Although the simulated value of the attenuation length or the inelastic mean free path is still uncertain, the theoretical results we presented above from two different models using the correlation G factor are based on the latest findings. So far, the two models do not differ significantly, however, our experimental result is closer to Tanuma's model.

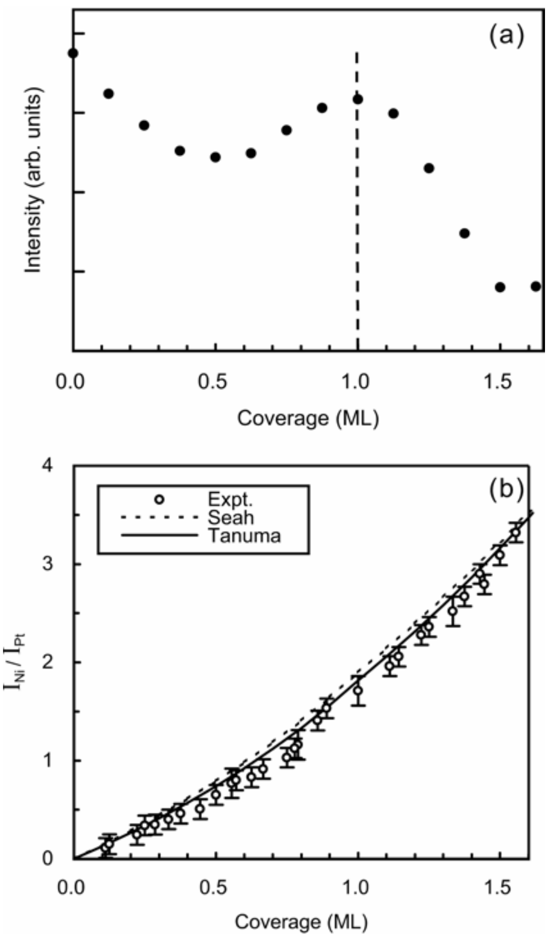

Fig. 3-6 (a) Intensity of the specular beam of LEED as a function of deposition time (I-t profile). A beam energy of 73 eV was used. (b) Comparison between experiments and theoretical calculations of Ni coverage deposited on Pt(111) surface. The Auger peak ratios of I_{Ni} / I_{Pt} are in better agreement with the prediction of Tanuma's model after G factor correction.

We further investigated a variety of chemical compositions at the interface by a depth-profile experiment. The 1.5 keV Ar ion energy was used for sputtering. The sample of 1.2 ML Ni/Pt(111) was pre-annealed for 30 minutes at 750 K and then cooled to room temperature before sputtering. Auger intensities of Ni and Pt versus sputtering time are shown in Fig. 3-7. After two minutes of sputtering, the Pt Auger signal decreased significantly and the Ni Auger signal increased slightly. These results show that the surface layers are occupied by Pt atoms due to the surface segregation during the formation of Ni-Pt alloy. After thermal annealing, the Pt enrichment in the surface layers is also observed in the system of Pt grown on Ni low index single crystal surfaces,[78] and Ni-Pt thin films grown on MgO(100) surface.[79] After further sputtering, the Ni Auger signal decreases and the Pt Auger signal increases sharply. All residual Ni atoms are removed after sputtering continued for 13 minutes. From the depth-profile study, one can show that Ni atoms diffuse into the Pt bulk after high temperature annealing.

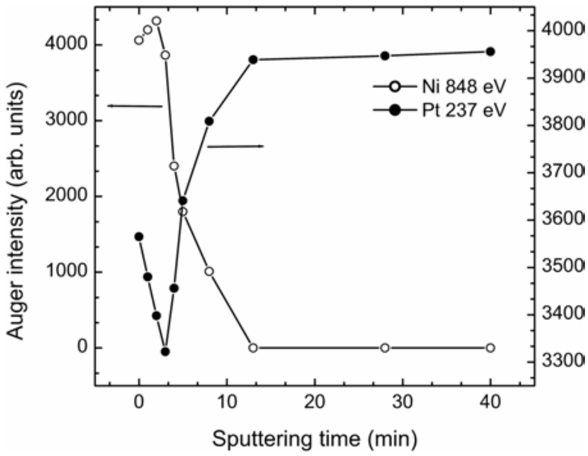

Fig. 3-7 Depth profile of 1.2 ML Ni/Pt(111) to monitor the intensity variations of Ni and Pt Auger peaks by 1.5 keV Ar^+ sputtering. The sample is performed after annealing at 750 K for 30 minutes.

UPS was used to monitor the evolution of the electron density of states in the Ni initial growth. The results are shown in Fig. 3-8a. The sharp Fermi edge and the d-band peak with a binding energy of 4.0 eV are observed on the clean Pt(111) surface. The peak heights of the Fermi edge and the *d*-band decline, and their peaks broaden gradually as the coverage of Ni increases. The binding energy of the *d*-band does not change when the coverage of Ni increases from 0 to 0.8 ML, but it shifts from 4.0 to 4.6 eV as the coverage of Ni increases from 0.8 to 1.4 ML. In order to observe the variations of these UP spectra more clearly, difference spectra (the spectrum of the Ni overlayer minus that of the clean surface) are also plotted in Fig. 3-8b. We plotted the height h_A of Fermi peak A (Fig. 3-8a) and the height Δh_B of the difference spectra at peak B (Fig. 3-8b) versus Ni coverage in Fig. 3-8c. These two curves are linear except for a sharp bend at 1.0 ML. The changes in the slopes are very significant. Due to the fact that the peak height or intensity of the UP spectra is similar to the Auger peak intensity, the magnitude of the received signals is proportional to the intensities from one specific chemical element. Therefore, peaks A and B coming from the mixture of the Ni and Pt signals are the only difference from the AES. Peak A has an ascending trend and Peak B has a descending trend. Hence, the two peaks are very surface sensitive and linearly correlated, each having a discontinuous kink in the growth of the adsorbate layer. The curves of h_A and Δh_B versus the coverage obtained from the UP spectra can be used to calibrate the coverage of the adsorbate and to determine the growth modes of thin films. Fig. 3-8c also shows that the initial growth from 0 to 1.4 ML is in a layer-by-layer growth mode. This conclusion agrees with the LEED observation in Fig. 3-6a.

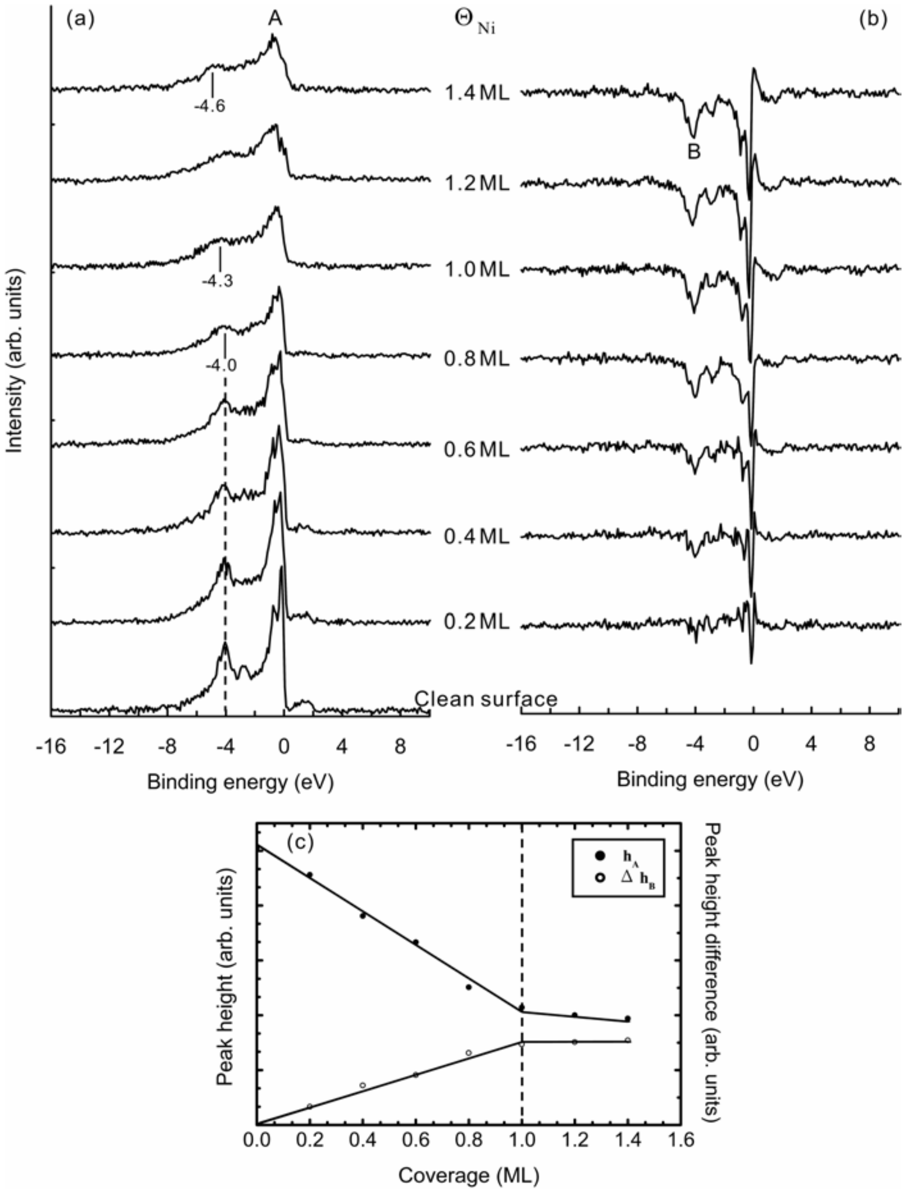

Fig. 3-8 (a) The variations of UP spectra versus the coverage of Ni. Peak A is located at the Fermi edge. (b) The corresponding UP difference spectra of Fig. 3(a). Peak B is the minimum in the d-band. (c) The height h_A of peak A, and the height Δh_B of the difference spectra at peak B as a function of the Ni coverage. Both h_A and Δh_B are clearly functions of the coverage of Ni and have sharp bends at 1.0 ML.

Further, the 1.2 ML of Ni on Pt(111) was annealed up to 750 K and observed the changes of the UP spectra at different annealing temperatures. The results are shown in Fig. 3-9a. The shape of the UP spectra has a significant change when the temperature exceeds 475 K.

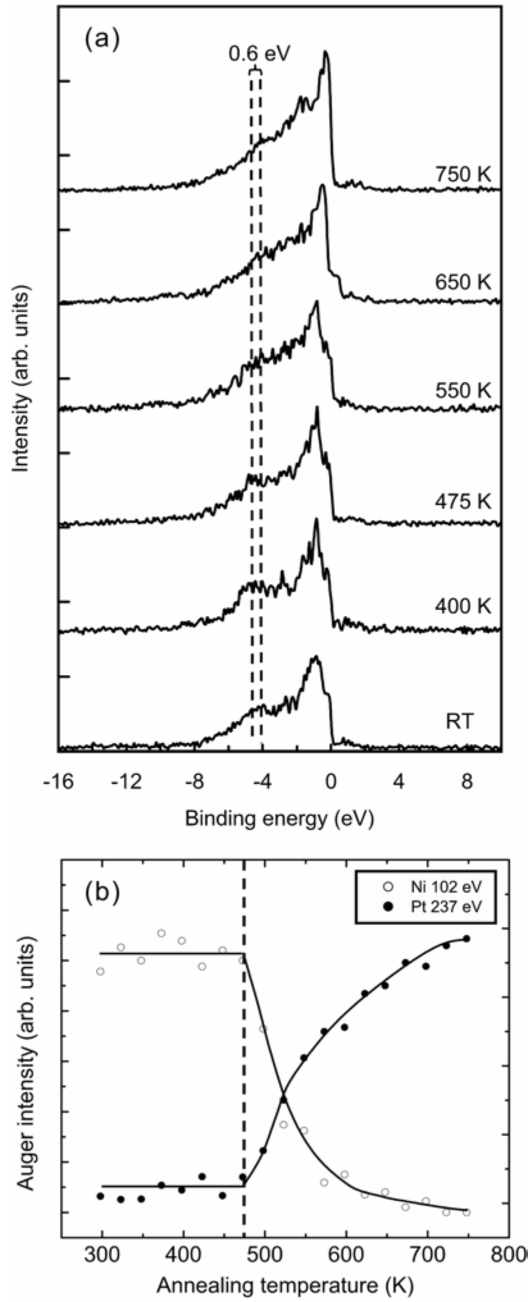

Fig. 3-9 (a) Evolution of the UP spectra for 1.2 ML Ni on Pt(111) versus the annealing temperature from RT to 750 K. (b) Ni and Pt Auger peak intensities as a function of annealing temperature for 1.2 ML Ni/Pt(111). The temperature of the formation of Ni-Pt alloy starts at 475 K. The continuous lines are a guide to the eye.

The *d*-band with a binding energy of 4.6 eV becomes flat and the peak height of the small bump at the Fermi edge gradually decreases. The peak of the *d*-band shifts back to 4.0 eV and the small bump at the Fermi edge disappears after the annealing temperature reaches 750 K. Comparing the 750 K annealed spectrum in Fig. 3-9a with that of pure Pt in Fig. 3-8a, it can be seen that there is a significant difference in the electronic states. This indicates that the high temperature annealing allows Ni atoms to diffuse into the Pt bulk to form a Ni-Pt alloy in the interface region and subsequently leads to the hybridization of the electronic states in the surface layers. In order to confirm the formation of the Ni-Pt alloy, the evolution of Ni MVV (102 eV) and Pt NNV (237 eV) Auger signals was monitored during the annealing process. The result is shown in Fig. 3-9b. The signal of Ni MVV (102 eV) is more surface sensitive than that of the Ni LVV (848 eV). This is the reason that we choose to observe the process of alloy formation. The alloy formation of Ni on Pt surface occurs at about 475 K. The diffusion of the Ni atoms toward the Pt bulk is rapid when the temperature increases from 475 K to 600 K. The diffusion is nearly complete at 750 K. According to the STM experimental results of Ni deposition on Pt(997), surface alloying at terrace and at step sites occurred even at below room temperature.[80] A high-Miller-index stepped plane usually has a high probability for the diffusion of atoms. In our studies, the Ni atoms diffuse toward the flat Pt(111) substrate. The Ni atoms must gain enough thermal energy to overcome the diffusion barrier for the flat Pt(111) surface. This may be the reason why the formation of Ni-Pt alloy needs a higher temperature than that of the stepped surface.

Seah's model and Tanuma's model were used to calculate the coverage of Ni on Pt(111) within 1.6 ML. Our experimental results closely match the Tanuma's model. The chemical composition, which showed enrichment of Pt atoms in the surface layers, was analyzed by a depth profile experiment after high temperature annealing. UPS was also used to observe the electron band structure which depends on the coverage and annealing temperatures. From the peak height of the Fermi edge versus Ni coverage, we can conclude that the initial growth within 1.4 ML is that of the layer-by-layer growth mode.

3-3 Alloy formation of capping Ag ultrathin films on Ni/Pt(111)

Understanding of macroscopic properties of the metal-on-metal films influenced by their microscopic interfacial and electronic structures generally requires detailed experimental or theoretical studies. Ni-Pt systems including thin films, multilayers, and alloys have been investigated intensively because of their segregation phenomena,[81] interesting magnetic properties,[82] and catalytic reactions such as the process of hydrogenation for industrial purposes.[83] Besides, Ag-Ni alloy not only exhibits giant-magnetoresistance properties;[84,85] it can also be used as a strain-sensitive material for piezoresistive sensors.[86] Thus, a system containing three constituents of Ag, Ni and Pt is very intriguing for a study. Our recent experimental study showed that the starting temperature for Ni-Pt alloy formation increases as the Ni thin films turn into 3-D islands.[87] A theoretical study shows that the face-related segregation of Ni-Pt alloy is due to the competition between the surface energy and the elastic strain release.[88] Silver and nickel are essentially known for equilibrium immiscible and do not form any compound owing to the large positive heat of formation.[89,90] Ag/Ni superlattices can produce sharp interfaces with immiscible Ag and Ni elements at low temperatures,[91] but Ag/Ni multilayers can break up following the formation of Ag and Ni grains during thermal annealing.[92] Although numerous experiments have been performed on the Ag-Ni-based system as previously mentioned, published reports lack findings about the growth and structural properties in the monolayer range. The bulk lattice misfits as we know are large at about 15.7 % for Ag/Ni interface and 13.8 % for Ni/Pt interface. It is very interesting to study the initial growth and the structural changes in the Ag/Ni/Pt interfaces, especially in the alloy formation of this heterogeneous system.

In this section, Auger electron spectroscopy (AES), ultraviolet photoelectron spectroscopy (UPS), and low-energy electron diffraction (LEED) were used to observe the initial growth and alloy formation at the interfaces after a high temperature annealing. From these techniques, we observed the formation of Ag-Ni surface alloy and noted some interesting structural changes in the interfaces.

Ni ultrathin films grew initially on Pt(111) in a 2 ML layer-by-layer mode that subsequently turned into a 3-D island growth at room temperature.[87] After 1 ML of Ni grown on Pt(111) surface, Ag atoms were deposited on 1 ML Ni/Pt(111). Fig. 3-10 shows the Auger-uptake curve during the Ag deposition. In the time interval between 0 to 600 s, the relative Auger signals of Ag MMV (351 eV), Ni LMM (848 eV), and Pt NNV (237 eV) are following an approximately linear relation with deposition time. All these Auger signals versus deposition time change to an exponential behavior after t > 600 s. This indicates that the Ag overlayer on the 1 ML Ni/Pt(111) is in a layer-by-layer growth for only 1 ML, and then turns to a 3-D growth. This growth mode was double-checked by the oscillation in the intensity versus deposition time of the LEED specular beam.

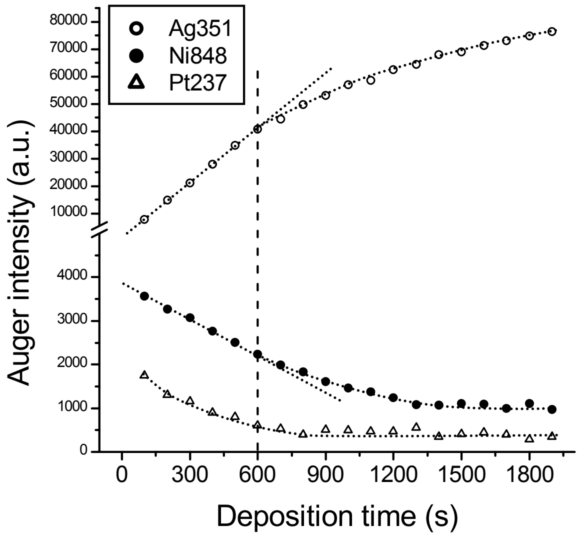

Fig. 3-10 The growth mode of Ag on the 1 ML Ni/Pt(111) was characterized by Auger signals versus deposition time (AS-t plot). Ag 351 eV, Ni 848 eV, and Pt 237 eV were used to observe the growth process. One turning point located at t = 600 s indicates that the growth mode changes to an island growth from 1 ML of Ag in a layer-by-layer growth.

The growth mode is mainly determined by the following two factors: lattice mismatch, and surface free energies including the interface energy. In our system, the lattice mismatch between Ag and Ni is very large (15.7 %); it favors the 3-D island growth. On the other hand, the surface energy difference $\Delta\gamma = \gamma_{Ag} + \gamma_i - \gamma_{Ni} < 0$ favors the layer-by-layer growth mode (γ_{Ag}=1.25 J/m^2, γ_{Ni}=2.45 J/m^2 and interface energy γ_i can be neglected).[93] With the competing lattice mismatch and surface free energy, the growth mode changes to 3-D growth after one monolayer of Ag grew in the layer-by-layer mode.

UPS is a powerful surface analysis tool of electronic structural identification. The evolution of the electronic structure in the valence band is interesting during the Ag film growth. He I ($h\nu$=21.2 eV) ultraviolet resonance radiation was used for the experimental light source. Only the photoelectrons in near normal emission were collected. We measured the UP spectra of different coverages of Ag grown on 1 ML

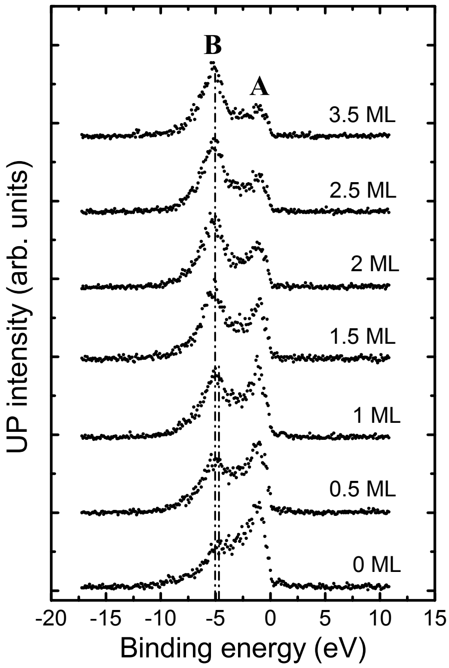

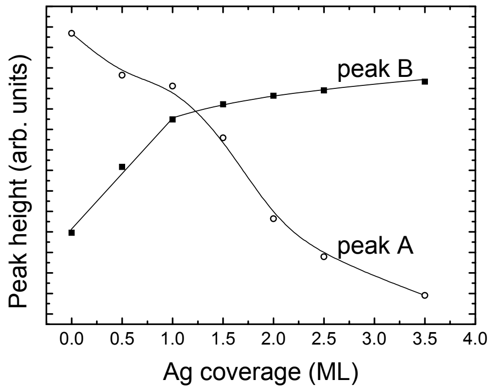

Fig. 3-11 (a) UP spectra varied with different Ag coverage on 1 ML Ni/Pt(111). Peaks A and B are the main peaks of the Ni-dominated and the Ag-dominated valence band, respectively. (b) The evolutions of the peak heights of main peaks A and B during the growth of Ag. The kink of peak B occurs at 1 ML of Ag coverage.

Co/Pt(111) as shown in Fig. 3-11a. The UP spectrum of 1 ML Ni on Pt(111) is shown in Fig. 3-11a labeling zero coverage (0 ML) of Ag. Ni-3*d* valence band mainly distributes between 0 and 2 eV, while Ag-4*d* band distributes between 4 and 7 eV below the Fermi level. These characteristic peaks are consistent with the recent report by Hite et al.[94] The sharp peak A is around the Fermi edge initially, and peak B enhances gradually when the coverage of Ag increases. In addition, peak B shifts from 4.7 eV to 5.1 eV when the coverage of Ag increases from 0 to 1.0 ML. However, peak B does not shift further when the coverage of Ag increases from 1.0 to 3.5 ML. The interaction between Ag-4*d* and Ni-3*d* states is weak because the Ag *d* band is full and these two peaks do not overlap.[95] The evolutions of peak A and B are shown in Fig. 3-11b. The height of peak A decreases gradually because the Ni enriched surface changes to the Ag enriched surface. Interestingly, the height of peak B becomes steeper when the coverage of Ag is between 0 and 1 ML. Then it becomes flat when the coverage is between 1.0 and 3.5 ML. The behavior is similar to our recent UPS study of Ni/Pt(111).[96] The discontinuous slope as a function of the coverage can be used to identify the growth mode and to calibrate the coverage of the overlayer in the initial growth. These results indicate that the UP spectra not only can be used for observing the electronic states near the Fermi edge in the submonolayer range, but also can be used effectively to calibrate the growth of thin films especially in a layer-by-layer growth mode.

AES is also a surface-sensitive tool used to observe the evolution of interface composition. Fig. 3-12 shows the Auger signals versus the sample temperature of 1 ML Ag/Θ ML Ni/Pt(111), where Θ=1-3. Each temperature was held for 10 minutes in annealing until the thermal equilibrium was reached. Fig. 3-12a shows the result of 1 ML Ag/1 ML Ni/Pt(111). Ag signals do not change apparently versus the sample temperature. Surface sensitive Ni MVV (102 eV) Auger signal starts to decrease at 500 K, while Pt Auger signal starts to increase. These results indicate that Ni diffuse into the substrate starting at 500 K to form Ni-Pt interface alloy. Interestingly, Ag atoms always stay on the top during the alloying process. The formations of Ni-Pt alloys including ordered, partially ordered and random alloys have been systematically studied.[97] Our early work in the 1 ML Ni/Pt(111) system showed that Ni atoms can start to diffuse into Pt substrate after about 450 K annealing.[87] The increase of the temperature for the formation Ni-Pt alloy after capping Ag overlayer indicates that the alloying formation needs more thermal energy to overcome the attractive interaction between Ag and Ni. Similar behaviors for 1 ML Ag/2 ML Ni/Pt(111) and 1 ML Ag/3 ML Ni/Pt(111) are shown in Fig. 3-12b and 3-12c respectively. The starting temperatures of the alloying increase to 610 K and 725 K, respectively. The higher temperature needed for the formation of Ni-Pt alloy in the thicker Ni films of 1 ML Ag/1-3 ML Ni/Pt(111) may result from high interface diffusion barrier of the strong Ni-Ni adatom interaction.

For further confirmation of alloy formation between the Ni-Pt interfaces with Ag overlayer, a depth profile by Ar ion sputtering was carried out as well. The variations of relative Auger signals of Ag 351 eV, Ni 848 eV, and Pt 237 eV versus sputtering time for 1 ML Ag/1 ML Ni/Pt(111) are shown in Fig. 3-13. Ar ion with kinetic energy 2.0 keV under 2×10^{-6} mbar was used for the depth profile experiment. The sample

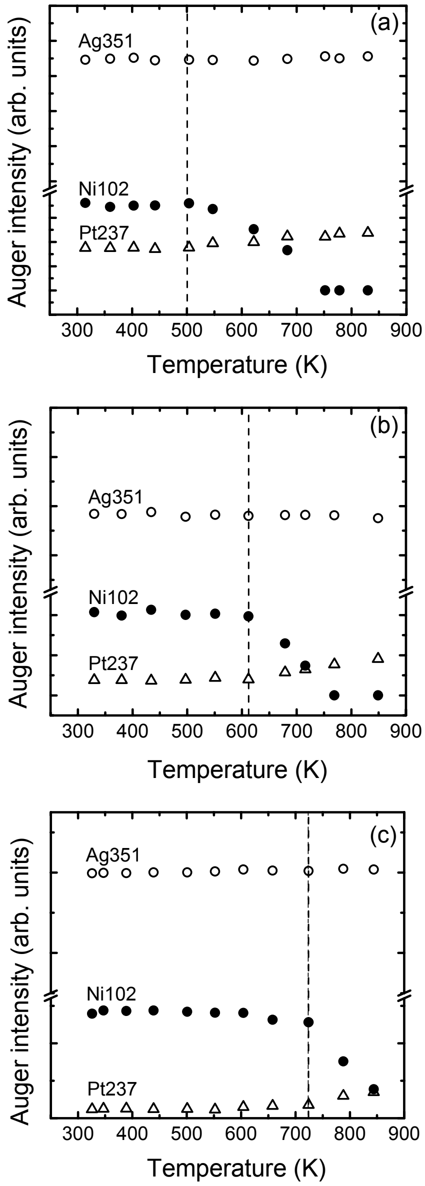

Fig. 3-12 The evolutions of Ag 351 eV, Ni 102 eV, and Pt 237 eV Auger signals as a function of annealing temperatures at different Ni coverages. Three samples are (a) 1 ML Ag/1 ML Ni/Pt(111), (b) 1 ML Ag/2 ML Ni/Pt(111), and (c) 1 ML Ag/3 ML Ni/Pt(111). The dash lines indicate the alloy formation of Ni-Pt occurred after these temperatures.

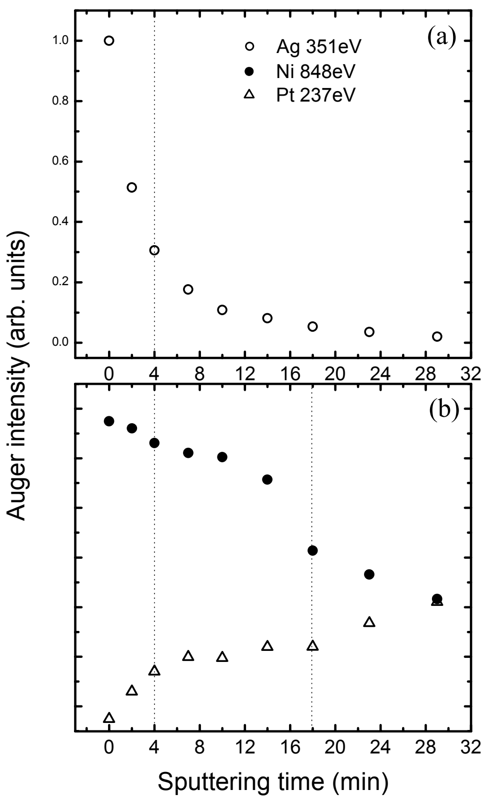

Fig. 3-13 The depth profile of 1 ML Ag/1 ML Ni/Pt(111) characterized by AES at room temperature after the sample has annealed at 800 K for 30 min.

was pre-annealed at 800 K for 30 minutes and then cooled down gradually to room temperature before the sputtering. Ag Auger intensities have been carefully checked during the annealing to rule out the occurrence of desorption from surface at a temperature higher than 820 K.[98,99] Ag Auger signal given in Fig. 3-13a declines very rapidly at the initial stage, while Ni Auger signal has a slight decrease and Pt Auger signal has a increase shown in Fig. 3-13b. Ag 351 eV signal always decreases until all Ag atoms have been removed, but Ni and Pt have a significant change in the time interval from 4 to 18 minutes. Ni-Pt based multilayers have a strong segregation effect after thermal treatment, and the Ni/Pt interface reveals a Pt-rich phase on the top surface.[88] Thus, after the Ag layers were initially removed in the time interval of 0 to 4 minutes, the Ni-Pt alloy with the Pt-rich phase is in the upper interface. In addition, we know that Pt 237 eV Auger signal is more surface-sensitive than that of Ni 848 eV. Thus, Pt Auger signal reveals a significant increase in the initial sputtering. After further sputtering, more Pt atoms are removed than that of Ni. This is why Ni Auger signal has a slight uplift in the time interval of 4 to 18 minutes. The decrease of Ni signal and the increase of Pt signal show an intermixing Ni-Pt alloy phase in the subsurface region after the sputtering of $t > 18$ minutes.

According to the depth profile in Fig. 3-13, the sputtering rate of Ag can be calculated from the following assumption. Assuming x is the removed percentage of Ag atoms after each sputtering, the Ag Auger signal I_N, which is proportional to the percentage of the residual Ag atoms after N sputtering, is calculated as $I_N = I_0(1-x)^N$, where I_0 is the Ag Auger signal before sputtering. After we plot the curve of $\ln(I_N/I_0)$ versus N, the sputtering rate of Ag is $x = 1 - e^L$, where L is the slope of the curve. The result is shown in Fig. 3-14. Note that each sputtering lasted 2 minutes. Interestingly, the slope changes at N = 2 (i.e. t = 4 minutes). The sputtering rate between $0 < t < 4$ minutes is 22.7%, but it decreases to 8.6% after $t > 4$ minutes. The change of the sputtering rate after 4 minutes of sputtering may indicate that small parts of Ag atoms reside on the topmost layer and the other Ag atoms intermix with Ni atoms in the second layer after high temperature annealing.

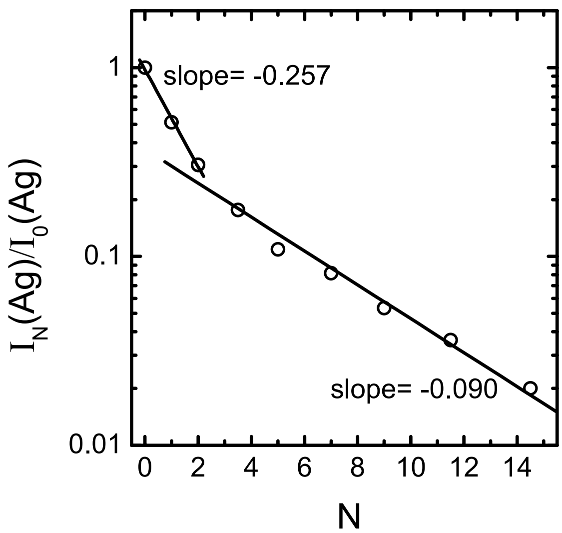

Fig. 3-14 The sputtering rate of removed Ag. It can be obtained from the slope of $\ln(I_N(Ag)/I_0(Ag))$ versus the sputtering numbers N. The vertical axis is in logarithmic scale.

For a further investigation in the structural change, we observed the evolution of LEED pattern during the high temperature annealing for 1 ML Ag/1 ML Ni/Pt(111). Although Ag thin layer on Ni(111) surface exhibits some interesting surface ordered structures,[100] we only observed a clear (1×1) hexagonal LEED pattern and no new structures were discovered in the growth of Ag on 1 ML Ni/Pt(111). This reveals that the growth of Ag overlayer is along the $<111>$-crystal axis. The diffracted spots of (1×1) pattern become fuzzy gradually during the high temperature annealing. Furthermore, a fine (2×2) LEED pattern was observed at room temperature after 800

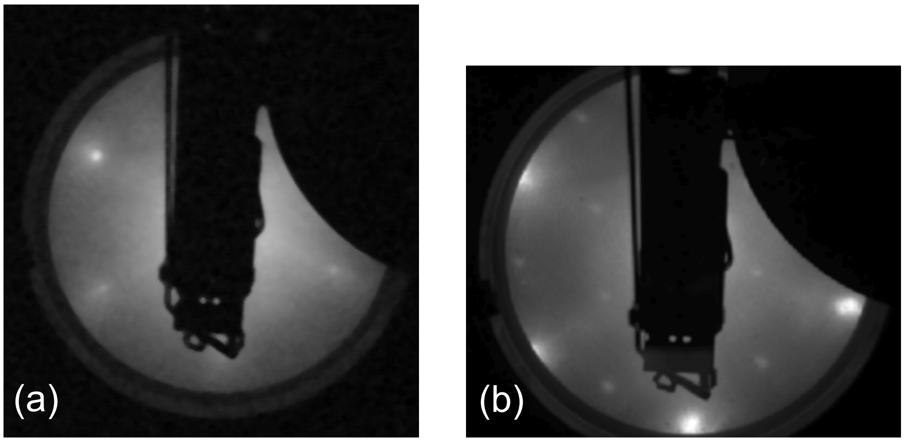

Fig. 3-15 LEED patterns show the surface structure of the 1 ML Ag/1 ML Ni/Pt(111). (a) as-deposited at RT (E=73 eV); (b) after annealed at 800 K (E=45 eV).

K annealing. LEED patterns of the as-deposited and the annealed sample are shown in Fig. 3-15. To our knowledge, this new surface structure has not been reported elsewhere. The coverage of Ag corresponding to the (2×2) ordered phase is 0.25 ML. Therefore, we propose that 0.25 ML of Ag with the (2×2) ordered structure exists on the topmost layer of the system. The second layer contains $Ag_{75}Ni_{25}$ (111) alloy and the remaining layers are Ni-Pt alloy. The schematic diagram of the possible interfacial structures is shown in Fig. 3-16a.

We further examined the structure of Ag-Ni alloys by a linear assumption of its lattice constant. Assuming the second layer of Ag-Ni alloy is homogeneous and using the bulk lattice constants, a_{Ag} = 0.409 nm and a_{Ni} = 0.352 nm, the lattice constant of $Ag_{75}Ni_{25}$ is 0.395 nm. It only differs from the Pt lattice constant, a_{Pt} = 0.392 nm, by 0.8%, as shown in Fig. 3-16b. After the high temperature annealing, the intermixing layer of the Ni/Pt(111) system is mainly Pt atoms from our previous UPS and AES studies.[96] Since the lattice mismatch approximates to zero, $Ag_{75}Ni_{25}$ alloy almost has no strain energy and becomes a stable alloy layer. Even with the complete immiscibility between Ag and Ni in the bulk phase, some Ag atoms may segregate along the interface to form the Ag-Ni alloy layer after high temperature annealing. This observation is identical to the annealing effect of Ag/Ni multilayers.[101,102]

From the Auger uptake study, the growth mode of Ag on 1 ML Ni/Pt(111) is layer-by-layer in the first monolayer, and then followed by the 3D islands growth. The evolution of UPS as a function of coverage confirmed the growth mode of the AES observation. It showed the density of states shifts from Ni 3d to Ag 4d band structure. The temperatures for Ni atoms diffusing into Pt substrate to form Ni-Pt alloy of 1 ML Ag /Θ Ni/Pt(111) are 500 K, 610 K and 725 K for Θ=1, 2, and 3 ML, respectively.

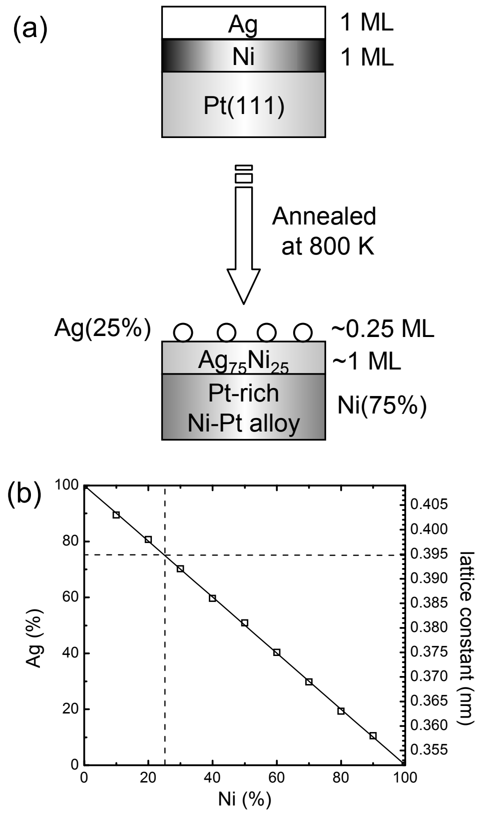

Fig. 3-16 (a) The schematic diagrams of the interface structures of 1 ML Ag/1 ML Ni/Pt(111) before and after the high temperature annealing. (b) The calculated lattice constants of the possible interface composition of Ag-Ni homogeneous alloy.

A new structural phase of (2×2) LEED pattern was observed when 1 ML Ag/1 ML Ni/Pt(111) was annealed at 800 K. From the depth profile experiment and the calculation of lattice constants, we propose that the interface structure of the annealed 1 ML Ag/1 ML Ni/Pt(111) is the 0.25 ML Ag in (2×2) structure on the topmost layer, followed by the $Ag_{75}Ni_{25}$ surface alloy in the second layer, and the remaining layers are the Ni-Pt alloy.

3-4 Magneto-optical properties of Ni/Pt(111)

Studying epitaxial metallic films and multilayers in view of their unusual magnetic and chemical behavior always attracted plenty of scientists devoted in the world. Ultrathin films and multilayers containing Co/Pd,[103-105] Co/Pt,[106-108] and also Fe/Pd,[109] and Fe/Pt,[110] have attracted considerable interest, because it was discovered that these multilayers exhibit a significant perpendicular magneto-crystalline anisotropy (PMA). Thus, studying the magnetic properties is usually one of the main focuses of researches on metallic macroscopic systems. In particular, such manufactured materials can be applied for ultrahigh-density magnetic recording media in the future.[111,112]

Nickel and platinum are chosen for study since Ni-Pt alloys have been studied extensively for well-known specific catalysis properties of industrial use The especially $Pt_{50}Ni_{50}$ alloy exhibits an important decrease in the chemisorption strength for molecular hydrogen and hydrocarbons.[113] The newest research even reported that monolayer Ni/Pt(111) surface can be also used as a new pathway of dehydrogenation and hydrogenation of cyclohexene.[114]

In equilibrium phase, Ni_xPt_{1-x} alloys are known to exhibit rich surface segregation.[115] In our earlier studies of Ni ultrathin film on Pt(111) surface, the Ni-Pt interface alloy formations have been discovered at high temperatures. The initial interface alloying temperatures of 0.8-3 ML Ni on Pt(111) are in the temperature range of 450-650 K. Although ultrathin Ni/Pt multilayers have been reported non-magnetic near room temperature small than 10 Å of Ni,[116] Ni/Pt multilayers have been found that room-temperature perpendicular magnetic anisotropy in the thickness range of Ni about 3.5-15 ML.[117] Due to its perpendicular anisotropy even at lower coverages (~2 ML) in the multilayer system[118] and lack of knowledge for Ni ultrathin film, we now have many interests to observe the magnetic properties in our epitaxial films of Ni on Pt(111) crystal. In the following, the magnetic properties by means of surface magneto-optical Kerr effect (SMOKE) technique were presented the θ_k as a function of coverage of the epitaxial growth Ni layers on Pt(111) and annealing effects experimentally.

It is known that the magnetic property of thin films is usually different from the bulk properties. The magneto-optic signal of ultrathin Ni film is hard to measure due to the weak magnetism. Thus, it possesses small Kerr rotation angle. We try hard to detect the weak MO signals down to 7 ML thin Ni layers at room temperature, but still obtain almost zero Kerr rotation. The result is consistent to the studies in Ref. 14. However, we believed MOKE signals would emerge from thick films of Ni. In Fig. 3-17a, the room-temperature polar and longitudinal hysteresis loops (M-H) curve as a function of coverage were shown with the increasing MO signals. After the coverage is over 8 ML, both directions from polar and longitudinal MO signals appeared. We observed clearly the P- and L- MOKE signals increase as increasing the coverage of Ni (Θ_{Ni}). The absolute value of Kerr rotation can be treated proportional to magnetization theoretically. When we measured the corresponding Kerr rotation (θ_k) in each hysteresis loop, we noted the Kerr rotation has just about 0.02º for 24 ML thicker layer of Ni. The Kerr rotation versus the coverage of Ni was shown in Fig. 3-17b. To prevent the systematic error with such small signals, we detected many

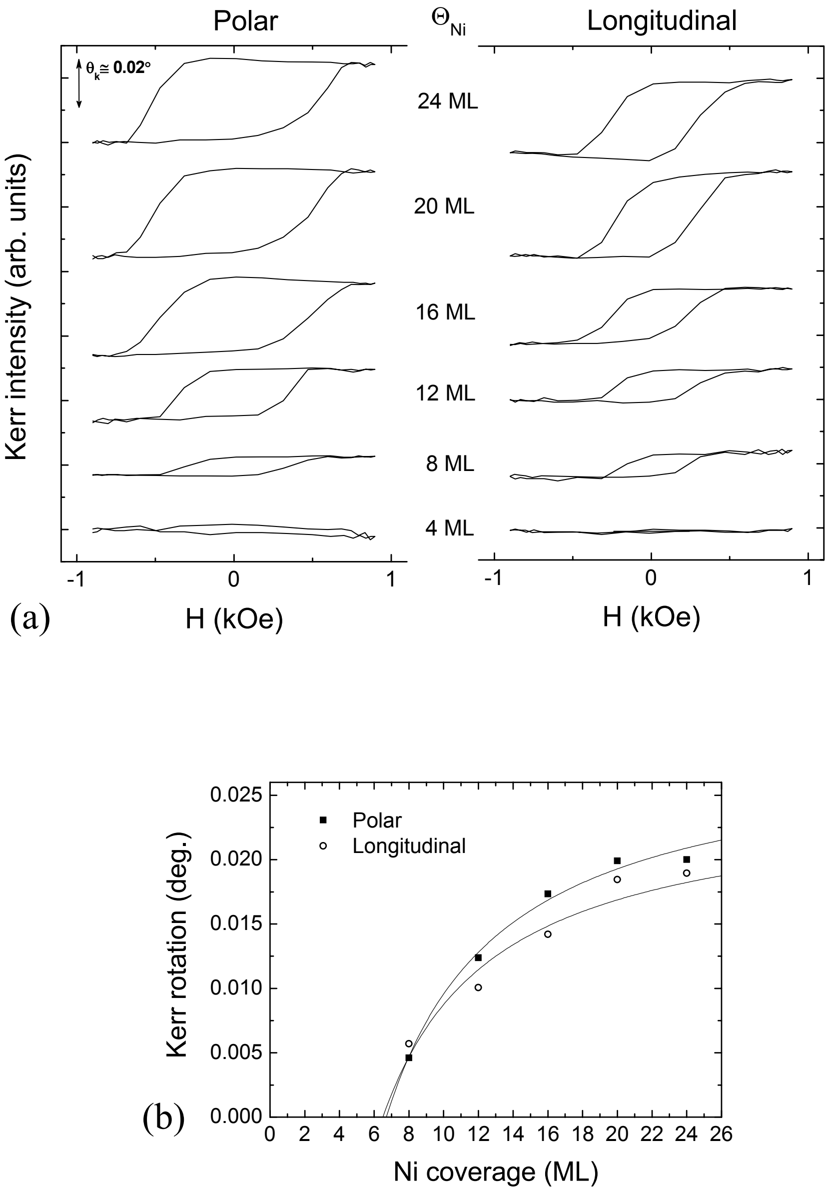

Fig. 3-17 (a) Polar and longitudinal hysteresis loops as a function of thickness for Ni films. (b) The saturated Kerr intensity as a function of thickness for Ni films. The solid line for fitting polar and longitudinal Kerr intensity was obtained using the relation of $M=M_0(1-\delta/\Theta_{Ni})$.

times in each measurement. It is worthwhile to point out that the nonlinear relationship between θ_k and the coverage of Ni shows a significant interfacial effect in the Ni-Pt interface. We believe that the magnetic moment of the Ni sublayer adjacent to the Pt sublayer is suppressed due to an overlapping between the *d*-band of Ni and the conduction band of Pt.[119] If we assume a simple relationship of the magnetization with the Ni coverage as the following equation:

$$M = M_0(1-\delta/\Theta_{Ni}) \tag{3-7}$$

Where M is the magnetization of Ni, M_0 is the saturated magnetization of Ni bulk, δ is the nonmagnetic layers of Ni at room temperature, and Θ_{Ni} is the coverage of Ni. Here, we consider that the magnetization is proportional to θ_k. Using this relationship we can well fit the dependence of the polar and longitudinal Kerr intensity in the Ni/Pt(111). The solid line was obtained from the Eq. 3-7 with the values of δ= 6.7±0.2 ML for polar θ_k and 6.5±0.5 ML for longitudinal θ_k. The result indicated that the nonmagnetic layers near room-temperature were estimated about 7 ML in error.

But one might ask a question, why the film thickness thinner than 7 ML near RT show nonmagnetic. The argument of the nonmagnetic layer is lasting for many years. As we know, the magneton number of Ni bulk (~0.606μ_B) is two or three times smaller than other ferromagnetic atoms (Co, Fe, etc.).[120] Recently some groups for the Ni/Pt system reported the possible mechanism is coming from the redistribution of electronic states between Ni and Pt. Its magnetic moment is even decreasing about 50% compared with its bulk values.[121] It may be due to the reduction of 3d holes for thin film was ascribed to a hybridization of the Pt and Ni *d* bands, resulting in a charge transfer from Pt to Ni *d* orbital. This is very similar with the result of thin Ni films on Cu(001).[122] Shin *et al.* once estimated the thickness of the nonmagnetic layer is about two atomic magnetic dead layers of Ni in the Ni/Pt multilayers system.[123] They conjecture that the magnetic dead layers come from suppression of Ni magnetic moments due to *sp-d* hybridization of Ni and Pt atoms at the interface. Nevertheless, Krakauer *et al.* suggested the Ni atoms at the interface where a narrowing of the d-band width and enhanced magnetic moments are expected.[124] By the contrary, the reduction in the density of states of *d*-band and boarder peak near the binding energy of 4 eV in the UP spectra may reduce the Ni moment.[125] That's why the MO signal of our system is so small and hard to measure.

Besides, from the structure point of view, it showed the coverage of Ni up to at least 6 ML maintains the horizontal strain and consequently shows a vertical spacing contraction (tetragonal distortion).[126] The stress in the surface layers may induce Ni different magnetic moments and the polarization of Pt. That's may be the other possible reason of the nonmagnetic Ni layers even down to 7 ML on Pt.

Fig. 3-18a shows the evolution of the hysteresis loops with annealing temperatures for 24 ML Ni layers on Pt(111). The Kerr signals decrease with temperature from RT to 661 K both P-MOKE and L-MOKE signals. We know that theories of magnetism in thin film are complemented by theories of the ferromagnetic monolayers, starting with the famous exact solution of the two-dimensional Ising model. The magnetization versus temperature follows the asymptotic power law[127]

$$M(T) = M_0(1 - T/T_C)^{\beta} \tag{3-8}$$

where M_0 is the magnetization at 0 K, T_C is the Curie temperature, and β is critical magnetization exponent. In general, $\beta = \frac{1}{8}$ of this model might therefore have a universal applicability in monolayers and ultrathin films. However, the problem is the extension of the critical regime. Now the model is used for our ultrathin film system. It can be clearly seen from a numerical fitting comparison with the $\theta_k(T)$ curve as given in Fig. 3-18b. Thus, we can obtain T_C=620 K and β=0.26 for P-MOKE and β=0.32 for L-MOKE. This magnetic critical exponents lie in between the XY model[128] and the 3D Heisenberg model.[129] The T_C is very close to the value from Ni bulk (627 K) that means the 24 ML Ni/Pt(111) film have revealed the bulk properties. Therefore, depositing the thinner layer of Ni might be a different behavior than 24 ML of Ni. When we compared the temperature dependence of magnetization with three different coverages 4, 12, 24 ML of Ni, we found the T_C shift forward lower temperature even down to RT. By using Eq. 3-8, we can calculate the fair values of T_C as 227 K, 507 K, and 620 K for the 4 ML, 12 ML, and 24 ML of Ni films, respectively. The experimental data and fitting curve are shown in Fig. 3-18c. The Kerr rotation for the 4 ML of Ni sample fluctuated seriously due to very weak Kerr signals. The result tells us that the T_C might be located at very low temperatures (0~200 K) in the ultrathin Ni film (1~3 ML). In our UHV system, the lowest value of temperature can be provided about 140 K. We can not measure the T_C lower than this value. That might be revealed nonmagnetic behavior in the atomic monolayer of ultrathin Ni. By this point of view the film lower than 7 ML without any MO signals near at RT is reasonable.

The magnetic property of Ni on Pt(111) was examined by P-MOKE and L-MOKE. The Kerr rotation for 24 ML Ni thin film is very small ~0.02º. From the simple assumption of nonmagnetic layer reduced the magnetization at the interfaces, we estimated the possible nonmagnetic Ni layers on Pt(111) about 7 ML at room temperature. The Kerr rotation emerged when the coverage is over 8 ML. Then the polar and longitudinal Kerr effect can simultaneously be measured. The Curie temperature measurements for 4 ML, 12 ML and 24 ML of Ni on Pt(111) surface is 227 K, 507 K and 620 K, respectively. Thus, we believed that Ni films thinner than 4 ML may possess lower T_C lower than 200 K or less.

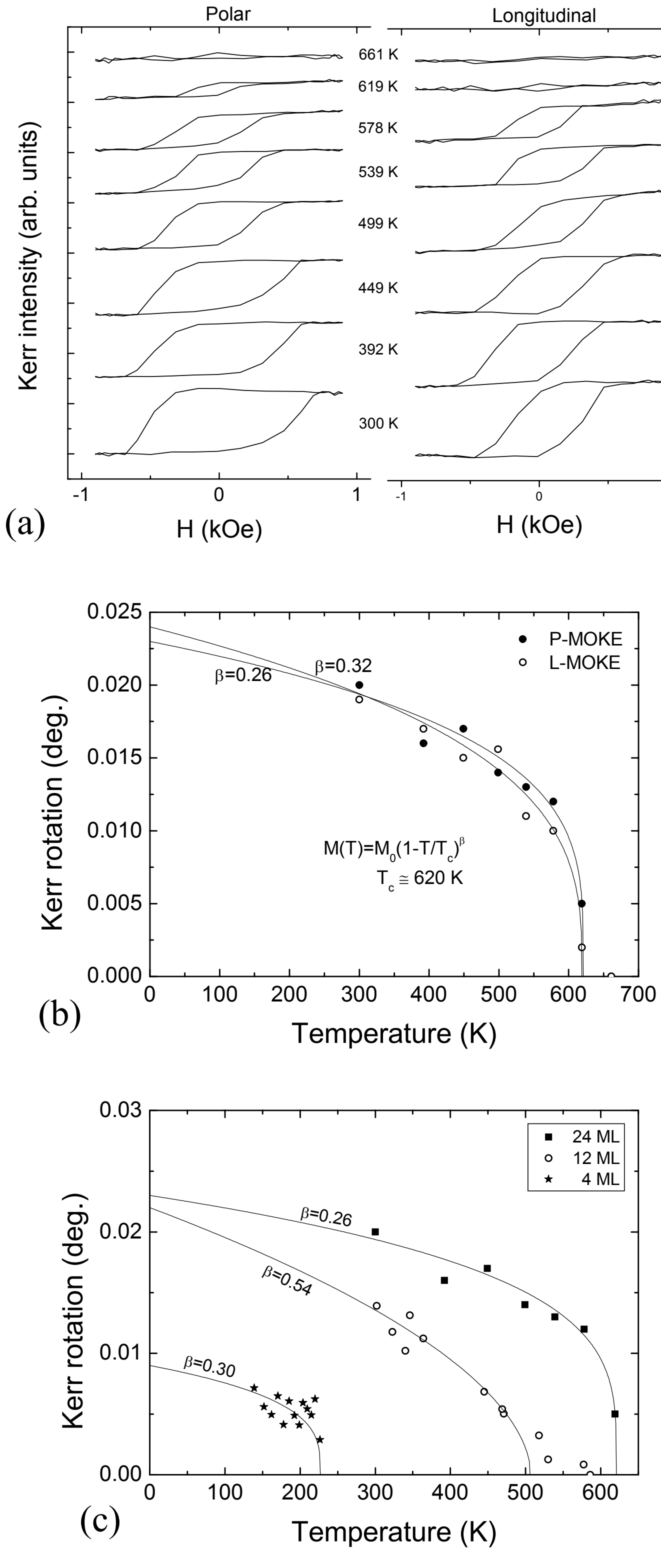

Fig. 3-18 (a) The evolution of polar and longitudinal hysteresis loops with temperature for 24 ML Ni/Pt(111) sample . (b) The Kerr rotation of 24 ML Ni/Pt(111) as a function of temperature was compared the asymptotic power low. (c) The temperature dependence of polar Kerr rotation for 4 ML, 12 ML, and 24 ML Ni/Pt(111), respectively.

3-5 Structure and Magneto-optic properties of Ni-based (Ni/Co/Pt and Co/Ni/Pt) ultrathin films

In recent years, Co/Pt multilayers and Co-Pt alloys has been extensively studied to be potential candidates for high-density magneto-optical recording.[130,131] The structure and the magnetic properties of ultrathin layers of Co/Pt(111) was found an enhancement of the perpendicular magneto-optical (MO) signals due to the alloy formation of Co-Pt after high-temperature annealing.[132-134] Interest in the coadsorption of the atoms of the two elements on crystal surfaces is increasing in recent because such studies open up new possibilities for producing surfaces with the required properties.[135]

Ni/Co heterostructures have an added interest due to the magnetic character of both constituent materials and lately they have attracted much attention. However, fewer reports for the atomic monolayer range of Ni and Co are presented. For the reason, both metals of Ni and Co are intriguingly chosen for studying their structural and magnetic properties in a monolayer range on the substrate of Pt(111). From the MOKE studies of Ni films on Pt(111) in section 3-4 of this paper, we believe that the low T_C of Ni films will alter its magnetic properties by intercalating strong perpendicular magnetic anisotropy (PMA) of Co layer in the Pt(111) system. Krishnan *et al.* have found the T_C of Ni/Pt multilayers with t(Ni)<1 nm is close to room temperature.[136] This result led us to the idea that by alloying Co with Ni could raise the T_C of the ML and indeed tailor it to suit any application. Therefore, for the lower T_C of Ni/Pt layers and the strong MO response of Co/Pt layers, it is undoubtedly provided a new opportunity for making new applicable materials. Thus, combined these layered materials has been the promising candidates for magneto-optical storage media. As our best knowledge, the T_C of Co-based multilayers which find application as magneto-optical recording media are much higher than the optimum writing temperature of about 200°C.[137] Because practical disk writing temperatures attainable with low-cost laser sources today are between 150 and 200°C.[138] Thus alloying Co with Ni has been projected as a variable solution to reduce the Curie temperature.

In this section, we presented the structural and magneto-optical properties of the ultrathin atomic layer of Ni and Co successively deposited onto the Pt(111) crystal surface. Our objective is to observe the alloy formations between Co–Pt and Ni–Pt and their corresponding MO properties affected by the two magnetic elements in the alloying processes. Author believes the competitive nature of magnetic properties might be very interesting. The structural properties of 1 ML Ni/1 ML Co/Pt(111) was first examined by AES, LEED, UPS and SMOKE. The SMOKE measurement in particular shows some unusual magneto-optical properties during high-temperature annealing. The enhancement of MO signals strongly corresponds to the different compositions of the structure, especially in the Co-Pt alloy, induced by thermal annealing. Except for the variation of the MO signals, Curie temperature (T_C) was more altered due to the addition of Ni. Then the mirror system of 1 ML Co/1 ML Ni/Pt(111) was also presented. Strong segregation of Ni located in the Co and Pt interfaces produced the low-T_C system. Moreover, the enhancement of the MO properties and coercivity were compared with 1 ML Co/1 ML Ni/Pt(111) system in this paper.

3-5-1 Structural properties of 1 ML Ni/1 ML Co/Pt(111)

Co films have been studied by STM at least 3 ML in a layer-by-layer growth mode on the Pt(111) surface,[8] but here we obtain a little difference in preparation of 1 ML Co layer on the Pt(111) crystal with faster deposition rates initially. The growth of 1 ML Co was re-checked by LEED and P-MOKE measurements. We first found small MO signals with small coercivity in the θ_k-H hysteresis (Fig. 3-19a) and spontaneously the fuzzy spots (Fig. 3-20a) as the 1 ML Co-layer deposited.

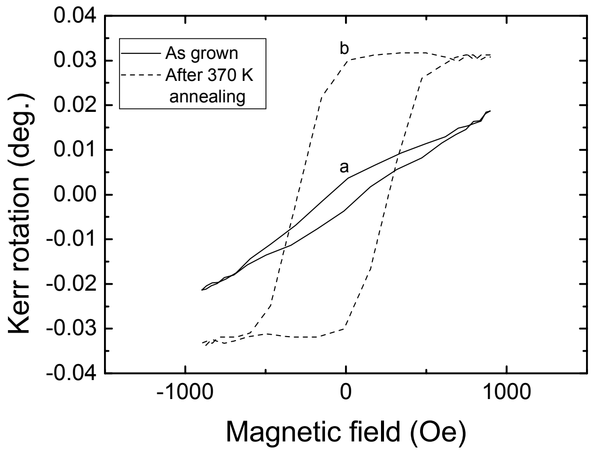

Fig. 3-19 The $\theta_k - H$ curve of 1 ML Co on the Pt(111) surface: (a) as-deposited and (b) after annealing at 370 K.

It is known that the growth mode is dominated by many factors like substrate temperature and deposition rate etc. The substrate temperature was kept accurately near the room temperature (300±3 K). However, faster growing rate of Co deposition about 0.2 ML/min may cause the structure of 1 ML Co/Pt(111) surface much different from that of lower rate (~0.07 ML/min) we have done before. Thus, the initial structure of 1 ML Co/Pt(111) can be treated as a rough surface with clusters. For this reason, we observed the structure of 1 ML Co on the Pt substrate again. Interestingly,

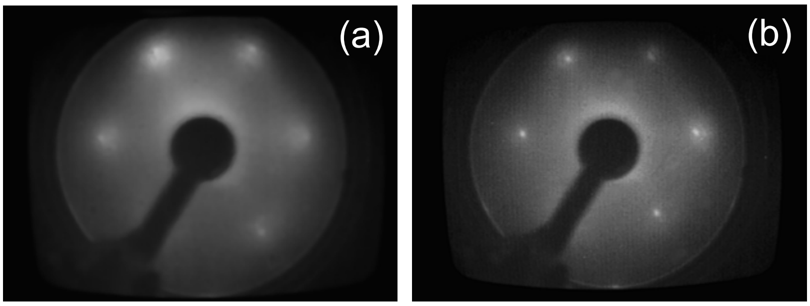

Fig. 3-20 LEED patterns of the 1 ML Co/Pt(111) surface. The pictures were captured (a) room temperature at E=116 eV and (b) after annealing at 370 K (E=125 eV).

we observed a structural phase transition by LEED which changes gradually from fuzzy spots at RT to sharper spots at about 370 K. On the other hand, the θ_k –H curve in Fig. 3-19b also show a significant increase in this range. The evidence indicates the rough-1 ML Co wets the Pt(111) surface around the annealing temperature of 370 K. Further, 1 ML of Ni was deposited onto the flattened 1 ML Co/Pt(111) surface as sample in this study.

The growing curve of Auger signals versus deposition time in Fig. 3-21a showed the growth mode of the Ni layer follows 2 ML layer-by-layer mode. The first kink of the slope corresponds to the first complete layer of Ni at 480 s. In Fig. 3-21b, the intensity evolution of LEED (00) beam during deposition also revealed two peaks in this oscillation curve at the same time in AES. The LEED pattern of the as-deposited sample did not show any new diffracted spot just (1×1)-structure, which means the adsorbed layers grow along the <111>-plane. Thus, the growth of Ni on the 1 ML Co/Pt(111) is following in a layer-by-layer mode up to 2 ML.

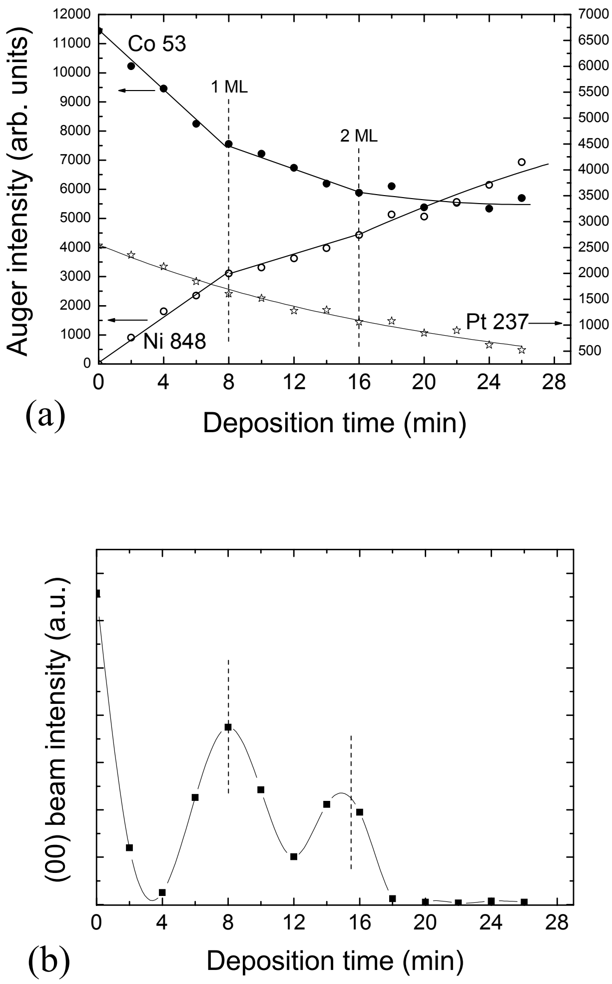

Fig. 3-21 (a) The growing curve measured by AES. Co 53 eV, Ni 848 eV and Pt 237 eV Auger signals were used for observing the growth of Ni on 1 ML Co/Pt(111). The kink between the bending slopes at 8 min and 16 min indicate two complete layer of Ni covered then island grows. (b) LEED (00) beam intensity during the deposition of Ni oscillates and has maxima at 8 min and 16 min.

3-5-2 Annealing effects for 1 ML Ni/1 ML Co/Pt(111)

The variation of surface compositions monitoring by the Auger signals during thermal annealing is an important topic in our experiment. In Fig. 3-22a and 3-22b, Auger signals of Pt 237 eV, Co 53 eV, 656 eV, and Ni 102 eV, 848 eV were all used for observing the change in the surface region. Co 53 eV and Ni 61 eV signals in Fig. 3-22b are very surface-sensitive than Co 656 eV and Ni 848 eV high-energy signals in Fig. 3-22a. In the initial annealing at 300~400 K, all signals did not have remarkable change until the annealing temperature reaching 440 K. The signal of Co 53 eV starts to increase and at the same time the signal of Ni 61 eV starts to decline. However, Pt

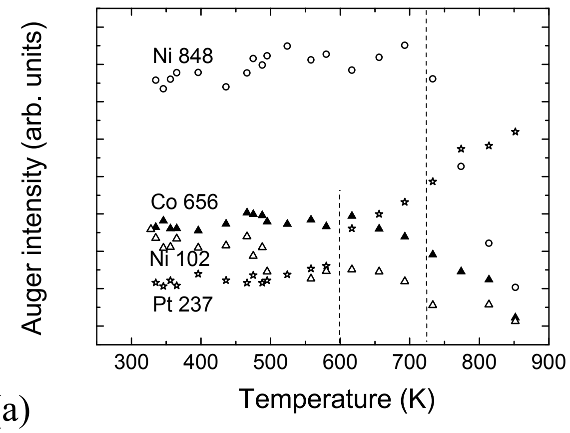

(a)

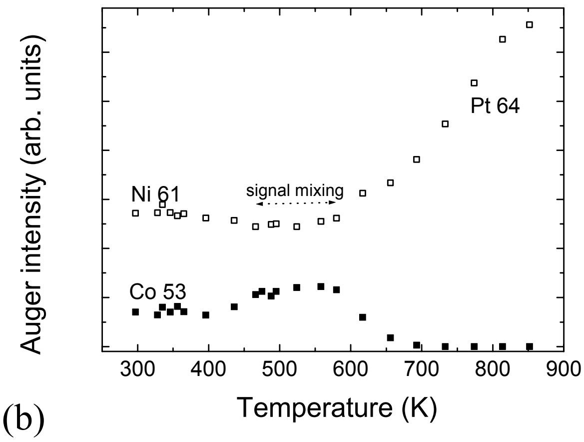

(b)

Fig. 3-22 The variation of Auger intensities of 1 ML Ni/1 ML Co/Pt(111) sample. (a) Pt 237 eV and Ni 102 eV Auger signals and high Auger electron energies of Co 656 eV and Ni 848 eV; (b) low Auger electron energies of Co 53 eV, Ni 61eV, and Pt 64 eV versus the temperature compared with (a) clearly show the differences of the surface sensitivity.

237 eV signals do not have marked change in the range. The possible structure is the mixing of the adsorbate in the upper interface between Ni and Co, but at the moment Ni and Co atoms do not diffuse into bulk of Pt. Further, the Co 53 eV signal drops rapidly and the Pt 64 eV signal has a rapid raise after the elevated temperature of 580 K. Pt 64 eV after 580 K can be clearly seen because its signals overlap with Ni 61 eV in the range of 475 to 560 K. According the earlier studies from the alloy formation of Co–Pt interface, this drop may possibly be corresponding to alloy formation that the Co atoms diffuse into the Pt bulk during the annealing. For Ni atoms, the obvious drop from surface-sensitive Ni 102 eV signals was observed until the annealing temperature of 600 K. The invariant Auger signals for the high-energy of Auger

signals of Co 656 eV and Ni 848 eV across these drop points can be treated as a strong proof of the alloy formation of Co–Pt and Ni–Pt not desorption of atoms. From the public database of NIST the inelastic mean free paths for the high-energy Auger electrons of Ni 848 eV and Co 656 eV are 13.2 and 11.4 Å, respectively, are longer than the low-energy of Co 53 eV and Ni 102 eV are 3.9 and 4.6 Å, respectively. The variation of Auger signals is very sensitive for lower energies near the surface layer, but for high energies the ejected signal coming from the deeper interlayer is preferred. Thus, the drop for the two non-overlapping Co 656 eV and Ni 848 eV high-energy Auger signals shifting to 650 and 700 K is reasonable.

3-5-3 Depth profile analysis for 1 ML Ni/1 ML Co/Pt(111)

The depth profile by ion sputtering can be effectively used for observing the chemical compositions normal to surface. The ion energy of the sputtering and the chamber pressure is 2 keV and 1.5×10^{-6} Torr. The surface-sensitive Auger signals of Co 53 eV, Ni 102 eV, and Pt 237 eV were recorded after each sputtering. The depth-profile experiment was performed at room temperature. Fig. 3-23 shows some significant modifications in the interface composition of 1 ML Ni/1 ML Co/Pt(111) after annealing at 750 K for 20 minutes. At the initial sputtering of 1 min in Fig. 3-23,

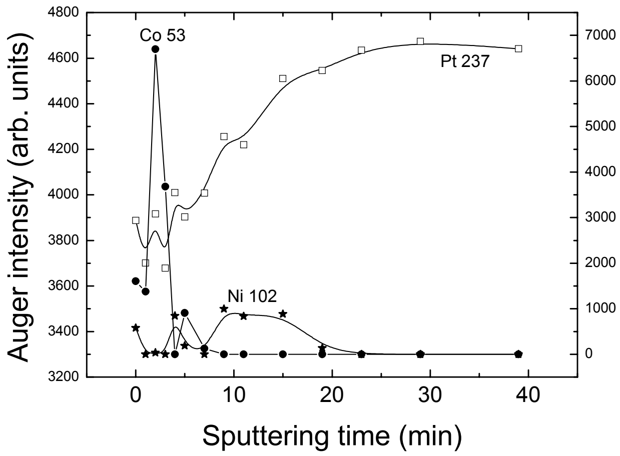

Fig. 3-23 The depth profile of 1 ML Ni/1 ML Co/Pt(111) after annealed at 725 K for 20 min. The surface-sensitive Auger signals of Co 53 eV, Ni 102 eV, and substrate signals from Pt 237 eV were used for observing the evolution of the surface concentrations.

Ni 102 eV and Pt 237 eV signals decreased rapidly but for Co 53 eV signals did not change obviously. That means the surface atoms may have some Pt and Ni atoms remaining on the surface. Then, Co 53 eV has a sharp increase at 2 min and a minor increase at 5 min. For Ni, 102 eV Auger signal has an increase at 4 min and a broader peak in 9-15 min. According the profile of the annealed 1 ML Ni/1 ML Co/Pt(111) sample, we can infer the existence of interface alloys of Co-Pt and Ni-Pt. Moreover, most of Co atoms stay at the upper surface than the Ni atoms. By contrast, the Ni layer located at the deeper interfaces. In other words, the deeper interfaces are dominated by Ni atoms.

In order to transform the relative Auger signals in Fig. 3-23 to corresponding chemical concentration, we used the following relation neglected matrix factors for the quantification of the depth profile which can be interpreted as[139]

$$x_A = \frac{I_A / s_A}{\sum_{i=A,B,C} I_i / s_i} \tag{3-9}$$

where x_A is the concentration for element A, I_A is the Auger intensity from element A, and s_A is the sensitivity factor of specific Auger transition from element A. The Auger sensitivity factor can be obtained from the reference table in the following page. One must be noted that the sensitivity factor would be divided by the corresponding Auger transition from the standard bulk value. Then the concentration of the depth profile for the annealed 1 ML Ni/1 ML Co/Pt(111) sample can be calculated as given in Fig. 3-24.

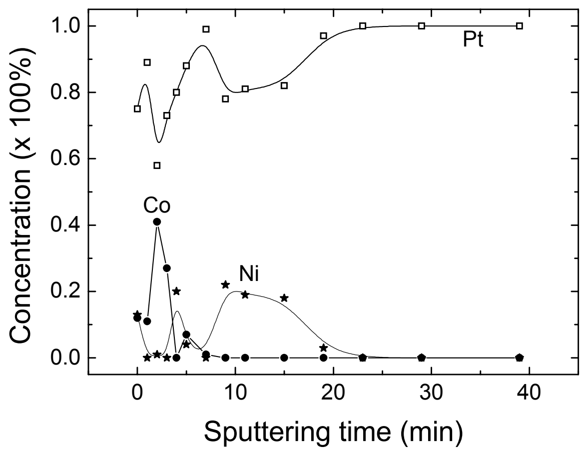

Fig. 3-24 The surface concentration of Co, Ni, and Pt for the 1 ML Ni/1 ML Co/Pt(111) sample after annealing at 725 K lasting for 20 min.

Ultimately, we obtained the possible $Pt_{75}Co_{12}Ni_{13}$ alloy in the initial condition. As the Ni and Co atoms diffuse into Pt bulk, the Pt-rich alloys are naturally formed.

Peak Positions & Sensitivity Factors for XPS & Auger Spectroscopy

(KLL=K; LMM=L; MNN=M)

	14 Si
<Atomic Number	14
Element Symbol>	Si
Kinetic energy, most intense Auger transition -{ 1621 K 0.266 / 96 L 0.924 }- PHI sensitivity factor for designated Auger electron transition	1621 K 0.266 96 L 0.924
Binding energy, most intense XPS transition -{ 102 2p3 0.283 / 153 2s 0.322 }- PHI sensitivity factor for XPS transition	102 2p3 0.283 153 2s 0.322

1 **H**																	2 **He**
3 **Li** 50 K 0.232 56 1s 0.025	4 **Be** 108 K 0.403 113 1s 0.074											5 **B** 185 K 0.391 191 1s 0.159	6 **C** 275 K 0.282 287 1s 0.296	7 **N** 389 K 0.600 402 1s 0.477	8 **O** 510 K 0.788 531 1s 0.711 23 2s 0.032	9 **F** 659 K 1.91 686 1s 1.000 30 2s 0.051	10 **Ne** 821 K 863 1s 1.340 41 2s 0.089
11 **Na** 996 K 0.282 30 L 0.528 1072 1s 1.685 64 2s 0.165	12 **Mg** 1188 K 0.405 48 L 0.649 90 2s 0.252 51 2p 0.124											13 **Al** 1396 K 0.390 70 L 0.655 74 2p 0.193 119 2s 0.288	14 **Si** 1621 K 0.266 96 L 0.924 102 2p3 0.283 153 2s 0.322	15 **P** 1862 K 0.183 123 L 11.38 133 2p3 0.412 191 2s 0.355	16 **S** 2119 K 0.111 153 L 2.43 165 2p3 0.570 229 2s 0.399	17 **Cl** 2395K 0.108 184 L 6.42 199 2p3 0.770 270 2s 0.441	18 **Ar** 219 L 241 2p3 1.011 319 2s 0.469
19 **K** 2979 K 0.030 252 L 0.716 293 2p3 0.870 378 2s 0.429	20 **Ca** 297 L 0.492 347 2p3 1.634 439 2s 0.527	21 **Sc** 343 L 0.625 402 2p3 1.678 501 2s 0.546	22 **Ti** 421 L 1.10 458 2p3 1.798 37 3p 0.239	23 **V** 475 L 1.01 515 2p3 1.912 40 3e 0.240	24 **Cr** 531 L 0.987 577 2p3 1.435 40 3p 0.241	25 **Mn** 592 L 0.599 641 2p3 1.582 48 3p3 0.254	26 **Fe** 705 L 0.663 710 2p3 1.791 55 3p3 0.301	27 **Co** 777 L 0.843 781 2p3 2.142 62 3p3 0.406	28 **Ni** 849 L 0.847 855 2p3 2.435 67 3p3 0.580	29 **Cu** 922 L 1.00 934 2p3 3.198 77 2p3 0.754	30 **Zn** 997 L 1.04 1022 2p3 3.354 89 3p3 0.870	31 **Ga** 1070 L 0.837 1117 2p3 3.341 105 3p3 0.972	32 **Ge** 1150 L 0.555 1219 2p3 3.100 31 2d5 0.408	33 **As** 1229 L 0.410 44 3d5 0.570 1326 2p3 2.103	34 **Se** 1311 L 0.120 57 3d5 0.722 232 3s 0.507	35 **Br** 1393 L 0.384 69 3d5 0.895 189 3p1 1.300	36 **Kr** 1478 L 88 3d5 1.096 216 3p1 1.394
37 **Rb** 1561 L 0.082 78 M 0.107 110 3d5 1.316 247 3p1 1.459	38 **Sr** 1651 L 0.100 114 M 0.108 133 3d5 1.578 280 3p1 1.536	39 **Y** 1748 L 0.107 132 M 0.281 158 3d5 1.867 313 3p1 1.621	40 **Zr** 1844 L 0.159 151 M 0.759 181 3d5 2.216 345 3p1 1.702	41 **Nb** 1944 L 0.115 170 M 0.707 206 3d5 2.517 364 3p3 1.186	42 **Mo** 2044 L 0.115 190 M 0.633 230 3d5 2.867 396 3p3 1.246	43 **Tc** 353 3d5 3.266 425 3p3 1.306	44 **Ru** 2256 L 0.084 277 M 1.13 282 3d5 3.696 463 3p3 1.349	45 **Rh** 2366 L 0.070 305 M 1.97 309 3d5 4.179 498 3p3 1.411	46 **Pd** 2476 L 0.065 333 M 2.04 337 3d5 4.642 534 3p3 1.437	47 **Ag** 2583 L 0.056 359 M 2.36 368 3d5 5.198 573 3p3 1.500	48 **Cd** 2694 L 0.040 379 M 2.61 405 3d5 3.444 618 3p3 1.542	49 **In** 2806 L 0.028 405 M 1.61 445 3d5 3.777 666 3p3 1.580	50 **Sn** 2919 L 0.023 432 M 1.73 486 3d5 4.095 715 3p3 1.618	51 **Sb** 3035 L 0.026 458 M 1.95 530 3d5 4.477 34 4d5 1.129	52 **Te** 3151 L 0.020 486 M 1.26 575 3d5 4.925 43 4d5 1.388	53 **I** 510 M 1.07 619 3d5 5.337 50 4d5 1.622	54 **Xe** 537 M 672 3d5 5.702 65 4d3 1.934
55 **Cs** 572 M 0.247 724 3d5 6.032 75 4d5 2.246	56 **Ba** 603 M 0.264 780 3d5 6.361 90 4d5 2.627	57 **La** 634 M 0.220 834 3d5 7.708 101 4d5 2.229	72 **Hf** 1625 M 0.262 17 4f7 2.221 213 4d5 1.520	73 **Ta** 1680 M 0.298 25 4f7 2.589 229 4d5 1.595	74 **W** 1737 M 0.298 34 4f7 2.959 245 4d5 1.657	75 **Re** 1793 M 0.259 43 4f7 3.327 263 4d5 1.739	76 **Os** 1850 M 0.204 52 4f7 3.747 279 4d5 1.819	77 **Ir** 1909 M 0.206 62 4f7 2.402 297 4d5 1.901	78 **Pt** 1969 M 0.191 73 4f7 2.709 316 4d5 1.967	79 **Au** 2022 M 0.184 85 4f7 2.964 336 4d5 2.081	80 **Hg** 2078 M 0.119 100 4f7 3.320 359 4d5 2.165	81 **Tl** 2132 M 0.095 118 4f7 3.669 385 4d5 2.239	82 **Pb** 2188 M 0.150 138 4f7 4.004 413 4d5 2.305	83 **Bi** 2243 M 0.062 159 4f7 4.383 443 4d5 2.419	84 **Po**	85 **At**	86 **Rn**
87 **Fr**	88 **Ra**	89 **Ac**															
				58 **Ce** 671 M 0.160 882 3d5 4.365 108 4d5 0.000	59 **Pr** 696 M 0.143 930 3d5 6.356 114 4d 2.224	60 **Nd** 734 M 0.177 980 3d5 4.697 120 4d 2.220	61 **Pm** 1034 3d5 3.754 129 4d 2.215	62 **Sm** 814 M 0.115 1083 3d5 2.907 132 4d 2.213	63 **Eu** 860 M 0.118 1136 3d5 2.653 136 4d 2.210	64 **Gd** 1030 M 0.108 1186 3d5 1.432 141 4d 2.207	65 **Tb** 1078 M 0.079 150 4d 2.201	66 **Dy** 1127 M 0.073 154 4d 2.198 293 4p3 0.673	67 **Ho** 1127 M 0.096 161 4d 2.189 306 4p3 0.670	68 **Er** 1228 M 0.080 169 4d 2.184 320 4p3 0.665	69 **Tm** 1452 M 0.143 180 4d 2.172 333 4p3 0.662	70 **Yb** 1511 M 0.172 185 4d5 2.169 342 4p3 0.660	71 **Lu** 1568 M 0.187 197 4d5 2.156 359 4p3 0.656
				90 **Th** 2634 M 0.025 335 4f7 7.498 677 4d5 2.963	91 **Pa**	92 **U** 2764 M 0.030 380 4f7 8.476 739 4d5 3.110	93 **Np** 402 4f7	94 **Pu** 427 4f7	95 **Am** 449 4f7	96 **Cm** 473 4f7	97 **Bk** 498 4f7	98 **Cf** 523 4f7	99 **Es**	100 **Fm**	101 **Md**	102 **No**	103 **Lr**

3-5-4 Magneto-optic properties of 1 ML Ni/1 ML Co/Pt(111)

The magnetic properties of 1 ML Ni/1 ML Co/Pt(111) during annealing was studied by polar magneto-optical Kerr effect (P-MOKE). We first noted that no L-MOKE signals were detected due to strong perpendicular magnetic anisotropies dominated by Co/Pt and Ni/Pt ultrathin films in a monolayer range. On the basis of ab initio calculations it has been predicted and experimentally verified that the presence of an interface between ultrathin close-packed layers of Co and Ni is sufficient to give rise to a large perpendicular magnetic anisotropy.[140]

The temperature dependence of the Kerr rotation is shown in Fig. 3-25. The Kerr rotation shows a slight increase in the range of 400 and 480 K and has a significant increase in 560 to 620 K. First, we know that the Kerr rotation θ_k is proportional to the magnetization of thin films. Normally, the magnetization of the system decreases with the temperature. In other words, the θ_k should follows the M(T) curve. The increases in the temperature ranges may be attributed to the modification of physical properties, especially for the structure. Interestingly, these changes just correspond to the changes of chemical compositions by AES. In the above mentioned of Fig. 3-22, we inferred the upper Ni layer intermixes with Co at around 400~480 K and the alloy formation of Co-Pt occurs in the annealing temperatures between 560 and 620 K. Further, the θ_k decrease rapidly as the annealing temperature higher than 660 K and approach to almost zero at about 720 K. Although one can treat this point of the temperature is the Curie temperature. We must note that the system of Ni/Co/Pt system has not been a layer-by-layer system but an intermixing Ni-Co-Pt alloy-layered system. The alloy formation of Co-Pt has been early found extensively an enhancement of the P-MOKE signal.[141,142] The polar Kerr rotation of the alloyed film is two times larger than that of the as-grown layer. In order to maintain sufficient magnetization of the multilayer, the surface cobalt content in the (Co,Ni) alloyed layer has to be kept relatively higher than that of Ni. This has been confirmed by our depth profile analysis. Though Co and Ni have almost similar lattice parameters, Co=3.544 Å and Ni=3.5239 Å,[143] it is reported that the magnetostriction constant λ_{100} of fcc Co-Ni alloys at room temperature increases while the magnetostriction constant λ_{111} marginally decreases with increasing Co content.[144] This may the another reason of the Co–Ni layer possessing a large polar Kerr rotation.

Furthermore, adding Ni layer may decrease the Curie temperature but for variable Ni content can obtain variable T_C values in the Co/Pt multilayer system.[145] For that reason, we rechecked the T_C of the annealed sample several times. The result is exhilarating because the T_C of the sample was shift to 670 K. That means the point in the first heating loop can not be directly inferred to the T_C of the annealed sample.

The T_C may be altered from the variable compositions of Ni-Co-Pt by annealing. Thus, when the sample was re-annealing up to 830 K for 20 minutes, we surprisingly found a much more shift forward the low T_C. Near room-temperature (325 K) T_C is clearly seen in the Fig. 3-25. We believe the low-T_C dominated by the compositional change of the alloy-layered structure. This finding is interesting and we believe this topic is worth for a broad study.

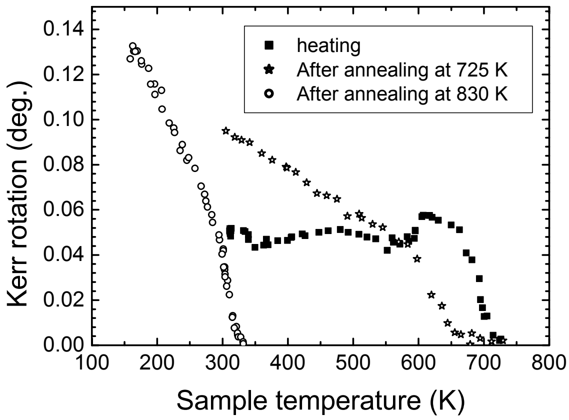

Fig. 3-25 The Kerr rotation as a function of sample temperature for 1 ML Ni/1 ML Co/Pt(111). The structure changes corresponding to different T_C by different annealing temperatures were clearly observed. Besides, the heating process was interpreted in the figure.

LEED is a very powerful technique and possesses a fast data acquisition in the determination of thin film structure. All LEED patterns were recorded near room temperature because LEED pattern becomes indistinct with strong background at high temperature and hard to record. As for the magnetic properties mentioned above, we observed the corresponding LEED patterns at some specific annealing temperatures. First, we found a special structure at T_a= 650 K, the order satellite spots surround each (1×1) 1st order spot in 3-fold symmetry were clearly seen in Fig. 3-26a. However, the LEED diffracted spots after annealing at 725 K become darker and fuzzy (Fig. 3-26b). After further annealing at 830 K, the 3-fold (1×1) 1st spots become more sharp and brighter. That means the alloy-layered quality improved after high-temperature annealing. According to the AES and P-MOKE studies, we can further explain the structure determined by LEED in Fig. 3-26. From the earlier compositional analysis of 1 ML Co-Pt(111) alloy surface by Tsay *et al.*,[146] the topmost and the second layer both may contain 50% of cobalt after annealing at 600 K. In general, forming these order satellite spots may be attributed to the following two reasons: (i) the lattice misfit exists between the upper surface layer and the lower surface layer or (ii) different domains forming at the top surface. The annealed 1 ML Ni/1 ML Co/Pt(111) surface containing the surface alloys of Co-Pt and Ni-Pt with Pt enrichment has been confirmed by the depth-profile experiment. From the depth profile of the layered structure, it is shown that most of the Co atoms locating at the upper layers. After a linear assumption of the lattice constants for $Co_{1-x}Pt_x$ alloys, the lattice parameters can be simply calculated by the bulk lattice constants of Co (3.55 Å) and Pt (3.92 Å). It is found the values close to the lattice parameter of the $Co_{50}Pt_{50}$ alloy, and in agreement with the depth-profile analysis of pure monolayer Co-Pt(111) by Tsay *et al.*[146] However, high annealing temperatures exceeding 700 K will destroy the surface symmetry of which the 3-fold order satellite structure observed by LEED. The patterns shown in Fig. 3-26b and Fig. 3-26c were captured after 700 K and 830 K, respectively. We believe that the Ni atoms may not diffuse too deep in depth by annealing at 650 K. The formation of ordered surface alloy shown in Fig. 3-26 is possible. The structure does not occur at the pure Co-Pt(111) system. In other words, adding Ni layer may contribute to the formation of layer-ordered phase. Nevertheless, more Ni atoms will diffuse deeply into the bulk when the annealing temperature is over 650 to 830 K. The diffused content of Pt onto the surface relatively increases. Ultimately, the layered structure has been improved by high-T annealing at 830 K with an alloyed layer near the top surface. (Fig. 3-26c)

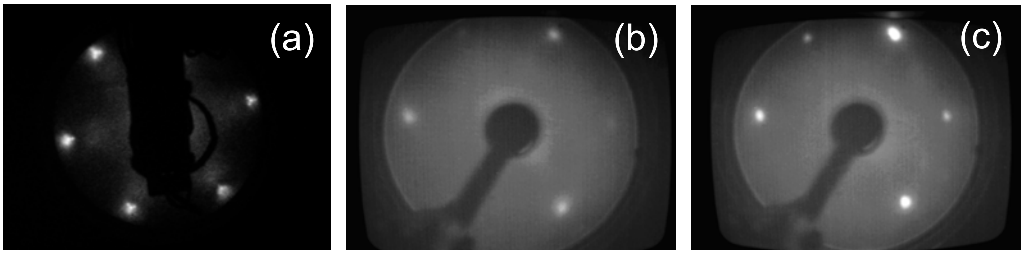

Fig. 3-26 LEED pattern of 1 ML Ni/1 ML Co/Pt(111) was measured at RT after (a) 650 K annealing at *E*=63 eV; (b) 725 K annealing at *E*=86 eV, and (c) 830 K annealing at *E*= 86 eV for about 20 minutes. The order satellite spots are clearly seen in (a). Other descriptions see in the article.

In this section, we found that the Ni capping layer in the Co/Pt(111) promotes the formation of microstructures and decreases the T_C of the Co/Pt ultrathin film system. In order to further study the role of Ni affected in the low-T_C system, we have prepared the pre-annealed 1 ML Co–Pt(111) alloy surface as the initial substrate. After that 1 ML of Ni film was then deposited onto the surface for observing the variation of magnetic properties at different annealing temperatures from 500 to 830 K.

First of all, the θ_k–T relation of the as-deposited 1 ML Co/Pt(111) and annealed Co-Pt alloy surface were shown in Fig. 3-27. A roughening transition of 1 ML Co layer from RT to 370 K was clearly seen. The alloy formation of Co-Pt begins at about 500 K and a grant enhancement around 670 K. According to the studies of Yamada et al.[147] and Harp et al.,[148] the possible enhancement of the θ_k may be contributed to the formation of the Co_3Pt alloy films. The Co_3Pt alloy films possess hcp order phase, with consisting of two kinds of layer: one layer consists of only Co atoms, whereas the other consists of the same amount of Co and Pt atoms. Harp et al. suggested the transformation temperature (T_{eq}) from hcp to fcc structure is about 650 K in Co_3Pt. That is why our M(T) curve show a maxima near 650 K. This result seems in agreement with our P-MOKE measurement. However, the Co atoms on the surface diffuse deeply into the bulk of Pt(111) change when the elevated temperature is over 700 K. The MO signals disappear rapidly at 720 K. We should note that this temperature is referred to the ordering temperature of the system. After these heating processes, we found that the T_C of the annealed 1 ML Co–Pt(111) sample is about 500 K. In order to explain the physical origin possessing the lower-T_C, the energy

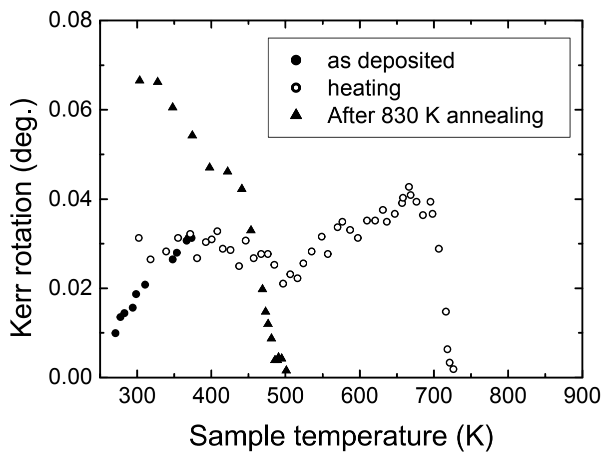

Fig. 3-27 The temperature dependence of the Kerr rotation of 1 ML Co/Pt(111). In this picture, three structural changes occurred: (i) smoothing effect from 270~370 K; (ii) the enhancement of Kerr rotation at about 670 K; (iii) after high-temperature 830 K. Other descriptions see in the text.

position of the peak in I(E) curve versus the index n^2 for the flattened-1 ML Co/Pt(111) before annealing and after annealing at 830 K is given in Fig. 3-28. According to the fundamental data of Co–Pt alloy phase the structure of the Co–Pt may be possibly close to $CoPt_3$ alloy.[149,150]

After 1 ML of Ni deposited on the 1 ML Co-Pt alloy surface, the heating cycles for the sample were running until five different annealing temperatures (T_a=500, 600, 700, 810, and 830 K) were reached for 20 minutes.(Fig. 3-29a) In the later, the sample was cooling down by slow rate (~0.3ºC/s) to RT for the MOKE measurement. The temperature dependence of the θ_k in principle follow the M(T) relation but the T_C

shifts to lower temperatures only when the T_a exceeds 500 K.

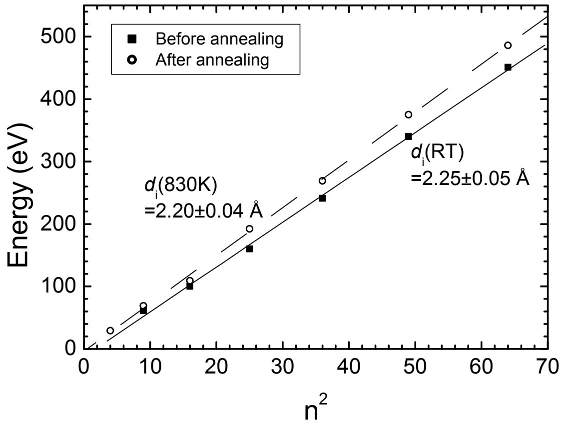

Fig. 3-28 The energy position of the peak of I(E) curve versus the index n^2 for the flattened-1 ML Co/Pt(111) before annealing and after annealing at 830 K for 20 min. The mean interlayer spacing of the annealed 1 ML Co/Pt(111) is shorter than that of non-annealed sample. This evidence can be also used to proof the interfacial alloy formations of Co-Pt.

Furthermore, the energy position of peaks in LEED I(E) curve was used for observing the variation of the mean vertical interlayer spacing (d_i). We compared the T_C value and the interlayer spacing of the annealed layer after each T_a (Fig.3-29b). The result indicates the d_i increases in the range of 500 to 700 K, the T_C then gradually saturate from 700 to 830 K to about 2.18 Å that is close to the Pt(111) surface spacing of 2.26 Å. We believed the alloy surface was a Pt-rich surface. The magnetic critical exponent β at different temperatures are larger then the 3D Heisenberg model (Fig. 3-29c). It implies that the annealed sample reveal 3-dimentional magnetic behavior. When we checked the relative chemical composition of Ni, Co and Pt by AES, we found an interesting result as given in the following Fig. 3-30. The evolution of relative Auger signals for Ni, Co and Pt was given in Fig. 3-30a. We chose high-energy Auger signals due to the limits of RFA-LEED which can not afford the information of low-energy range under 100 eV. We see the Ni 848 eV and Co 656 eV signals decreased with temperature, but Pt 237 eV increased much more when T_a > 700 K. That means the Pt atoms diffuse to the upper layers and form a Pt-rich surface especially at T_a=830 K. Due to the approximate 6 monolayers penetration for Ni 848 eV and Co 656 eV, we use Eq. (3-9) to estimate the mean surface concentration within six layers on the top surface.

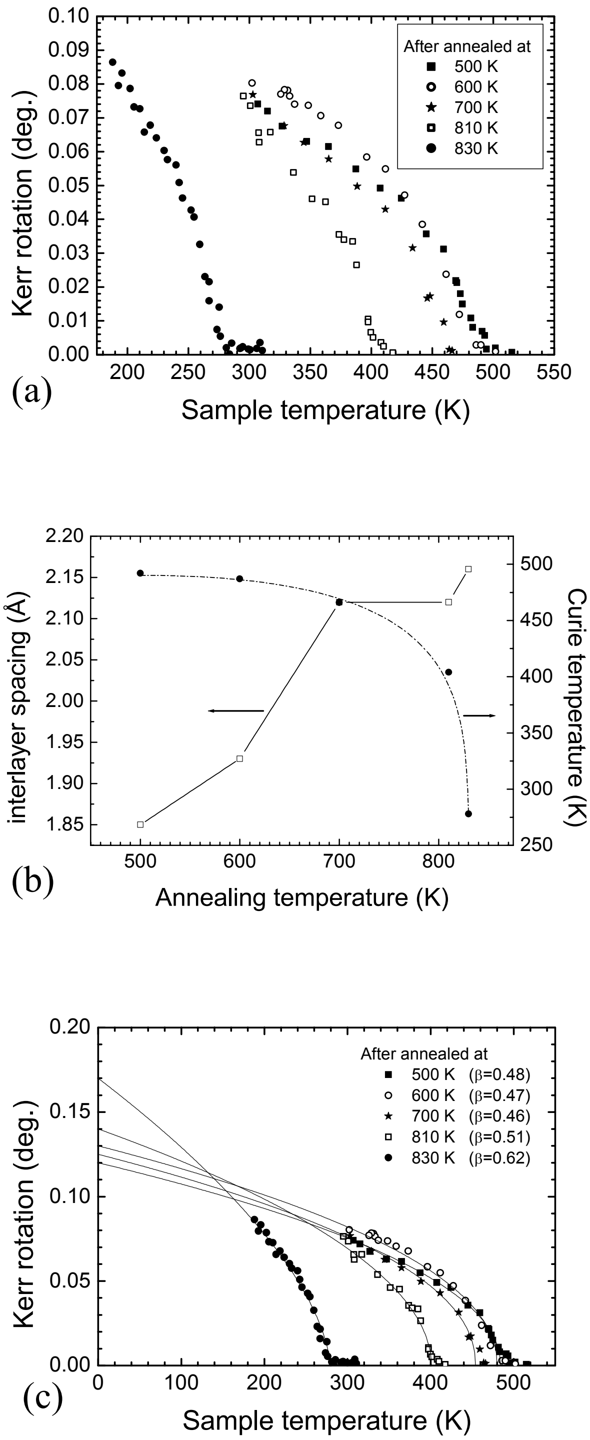

Fig. 3-29 (a) The temperature dependence of the Kerr rotation for 1 ML Ni/1Co-Pt alloy surface was measured by heating-cooling cycles after different annealing temperatures. (b) The Curie temperature and the corresponding mean interlayer spacing of the annealed sample are a function of the annealing temperature. (c) The solid line was obtained using the relation of Eq. 3-8.

The results of the calculation of the relative concentration are given in Fig. 3-30b. We are very surprising the composition of Co is invariant about 30% in the estimated surface region. This phenomenon can explain most of Co atoms did not diffuse too deep and just located at the surface few layers. But for Ni and Pt, a clear compositional variations from T_a=500 to 830 K defined the role of the intercalating Ni layer in the 1 ML Co–Pt(111) alloy system. Finally, we obtain the calculated

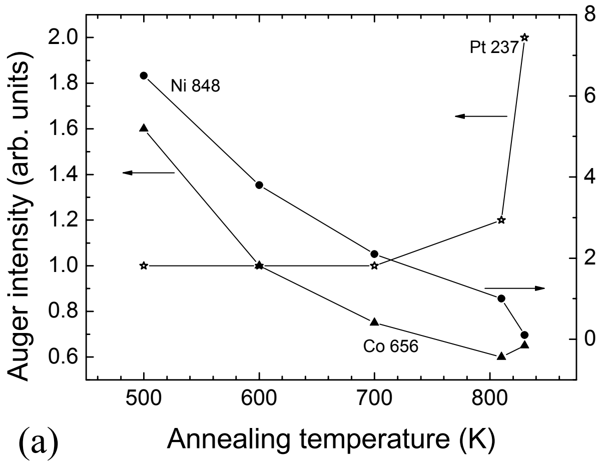

(a)

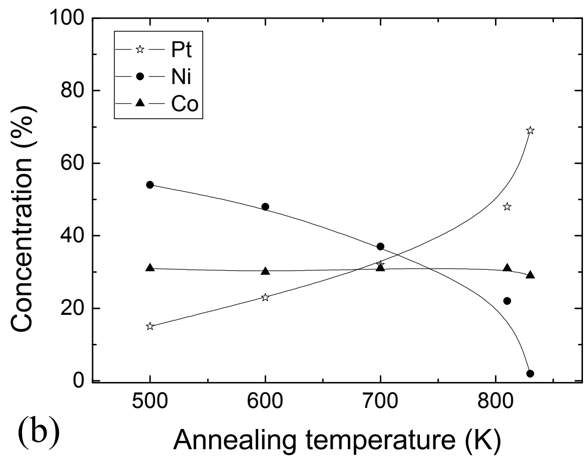

(b)

Fig. 3-30 The determination of the surface concentration for 1 ML Ni/1 ML Co–Pt(111) alloy sample. (a) The evolution of relative Co 656 eV, Ni 848 eV and Pt 237 eV Auger signals with annealing temperature. (b) Relative surface concentrations of Ni, Co and Pt in different annealing temperature. The surface becomes the Pt-rich surface in the top layers at T_a > 700 K.

$Pt_{0.69}Co_{0.29}Ni_{0.01}$ alloy after 830 K annealing. The diffusion volume of Ni and the segregation layer of Pt dominated the T_C and play an important role in annealed system. Poulopoulos *et al.* once reported the Pt_m-$[CoPt]_n$ multilayer revealing decrease of the Curie point when Co content decreases.[151] Namely, by different annealing conditions one may creative specific layer-alloyed structures and the low-T_C system.

3-5-5 Structural properties of Co/Ni/Pt(111)

The mirror system of 1 ML Co/1 ML Ni/Pt(111) was studied for a comparison. In the initial growth of Co films on Ni/Pt(111) we see without any oscillations just a exponential decay of intensity by LEED. The report from Rafaja *et al.* by means of glancing angle X-ray diffraction (GAXRD) shows that the huge mutual diffusion of Co and Ni leading to the destruction of the Co/Ni superlattice.[152] On the other hand, from the surface energy for Co γ_{Co} =2.79 J/m^2,[153] Ni γ_{Ni} =2.45,[154] 1.85 J/m^2,[143] and Pt γ_{Pt} =2.70,[154] 2.34 J/m^2,[143] Co film is still favor 3-dimentional growth in the Ni/Pt(111) than Ni film grows on the Co/Pt(111) surface.

In the composition analysis by AES, we see a very similar effect as compared with 1 ML Ni/1 ML Co/Pt(111) system. The alloy formation of Co-Pt and Ni-Pt were occurred at the high temperature annealing. In Fig. 3-31a, the clear transition temperature is located at the same positions of about 580 K, Auger signals for Co 656 eV and Ni 102 eV decreased across the line and simultaneously Pt 237 eV signal starts to increase. The signals for high Auger electron energy of Ni 848 eV drops at the higher T_a=725 K. We believed that the alloying effect took place as the annealing temperature over 580 K. Although the variation of Auger signals for Co 656 eV and Ni 848 eV without significant change before T_a=570 K, for the signals of low Auger electron energy Co 53 eV and Ni 61 eV have a significant change in the relative signals. Co 53 eV signals in Fig. 3-31b decline gradually and Ni 61 eV signals increase slightly in the temperature of 400 and 480 K. Then the Co 53 eV signals obviously drop rapidly at about 575 K. The two temperature ranges of 400 to 480 K and around 575 K should be noticed for the change of surface composition. In the temperature range of 400 and 480 K, we believe the two adsorbed layers are mixing each other at the top surface until the temperature is reached at 580 K both low-energy Auger signals of Co and Ni just decay after this temperature. In other words, the two atoms simultaneously diffuse into the bulk of Pt and the alloying effect of Co-Pt and Ni-Pt occurred after 580 K. Besides, the low energy of Auger signals is very surface-sensitive in the top surface region than that of the high energy of Auger signals. Thus, they are very suitable for composition analysis in the monolayer surface.

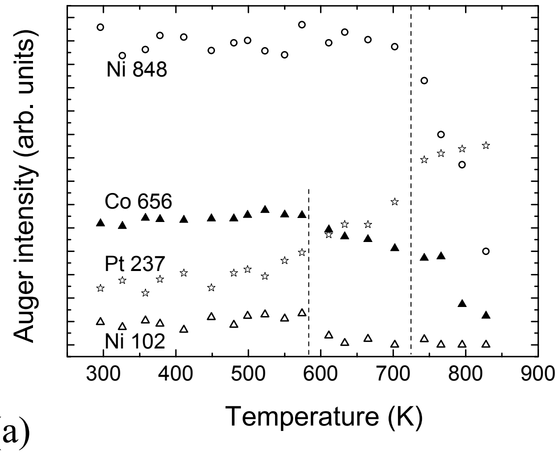

(a)

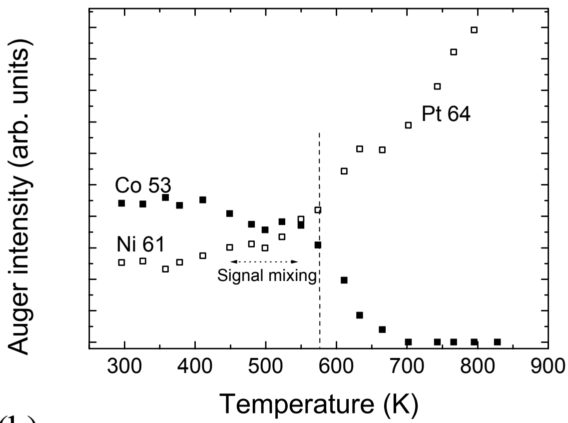

(b)

Fig. 3-31 The variation of Auger intensities of for 1 ML Co/1 ML Ni/Pt(111) sample. (a) Pt 237 eV and Ni 102 eV Auger signals and high Auger electron energies of Co 656 eV and Ni 848 eV; (b) low Auger electron energies of Co 53 eV, Ni 61eV, and Pt 64 eV versus the temperature compared with (a) clearly show the differences of the surface sensitivity.

3-5-6 Magneto-optic properties of Co/Ni/Pt(111)

The magnetic properties of 1 ML Co/1 ML Ni/Pt(111) were also measured by P-MOKE. The corresponding the θ_k - H curve is given in Fig. 3-32. The almost zero Kerr rotation initially can be treated as the island-like film morphology. In the earlier experiment in our studies, it has been mentioned that the island growth of 1 ML Co on Pt(111) may contribute to small MO signals. We first warm up the sample within 400 K to flatten the surface. But it is contrary to our expectation that the Kerr rotation still only has 0.01°. When the sample temperature increased, the θ_k raised rapidly from 400 to 470 K, it is very interesting that the temperature is just corresponding for the structural change of the mixing of Co and Ni in the top layer. According to the structure properties of Co/Ni/Pt, we believe the smoothing effect of Co and the mixing effect of Co and Ni enhanced the θ_k. The sample was then cooling down for the second time of the heating process. We then found the θ_k returned to about 0.06º. This result proved the mixing effect of Co and Ni is an irreversible process for magneto-optic property. Further, the θ_k as a function of temperature is following the behavior of the M(T) curve until the T_a was reached 660 K. The θ_k is down to zero at this temperature but in the latter an abnormal enhancement in the range of 670 to 720 K. This unusual phenomenon for the MO properties according the magnetic phase and structural studies of Co-Pt and Ni-Pt, this enhancement of the MO signals may be attributed to the CoPt alloy phase.[144] Although Co and Ni may form alloy with Pt at high T_a, the diffusibility of Ni seems larger than that of Co. From the depth profile experiment of 1 ML Ni/1 ML Co/Pt(111) after anneal, the Ni atoms indeed diffuse to deeper than Co. Thus, we suppose the diffusibility of Ni is higher than that of Co. So that in the Co/Ni/Pt layer, we believed the Ni layer underneath the Co layer may diffuse deeper than that of 1 ML Ni/1 Co/Pt(111) at 670 to 720 K. The more Co atoms may form an order phase with the segregated Pt atoms. Then the surface layer containing the $Co_{50}Pt_{50}$ ($L1_0$) alloy is possible and in agreement with the studies from Tsay *et al.*[146] So far, this possible inference seems reasonable, but it is still a question opening to a further study.

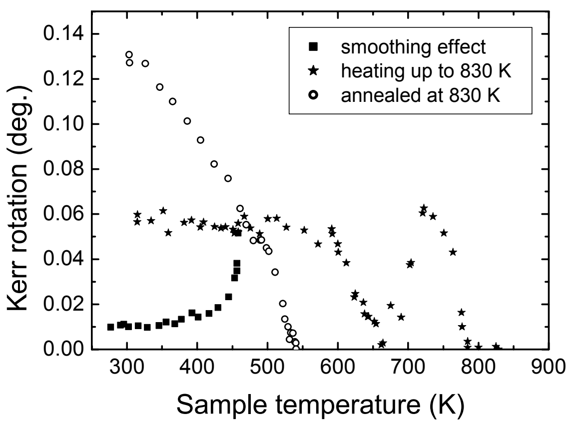

Fig. 3-32 The Kerr rotation θ_k versus the sample temperature for 1 ML Co/1 ML Ni/Pt(111) sample. With comparison of the θ_k-T curve of 1 ML Ni/1 ML Co/Pt(111), three points are very similar. (i) the smoothing effect in 270~460 K; (ii) the net magnetization approach to zero due to structural changes in 660~800 K. (iii) The T_C value shifts to about 540 K owing to Co and Ni diffusing into Pt bulk after high-temperature annealing at 830 K 20 minutes.

3-5-7 Comparative study for 1 ML Ni/1 ML Co/Pt(111) and 1 ML Co/1 ML Ni/Pt(111)

The room-temperature hysteresis loops of 1 ML Ni/1 ML Co/Pt(111) and 1 ML Co/1 ML Ni/Pt(111) sample were shown in Fig. 3-33. The MO signals increase slightly after adding Ni to the Co layer and the H_C did not change just a slight increase from 290 Oe to 310 Oe in the left of Fig. 3-33a. The huge changes occurred after 830 K annealing. The MO signals increase obviously in the 1 ML Co/Pt(111) and 1 ML Co/1 ML Ni/Pt(111) samples, but for 1 ML Ni/1 ML Co/Pt(111) we obtained the lower MO signal than that of as-deposited sample. The coercivity for the 1 ML Co/Pt(111) in Fig. 3-33a is increasing from 290 to 305 Oe but for the 1 ML Co/1 ML Ni/Pt(111) in Fig. 3-33c is increasing from 310 to 675 Oe. For the 1 ML Ni/1 ML Co/Pt(111) sample (Fig. 3-33b), the H_C decreased from 305 to 260 Oe. Author considers the possible physical reason may be coming from the residual compositions of Co and Ni on the top surface.

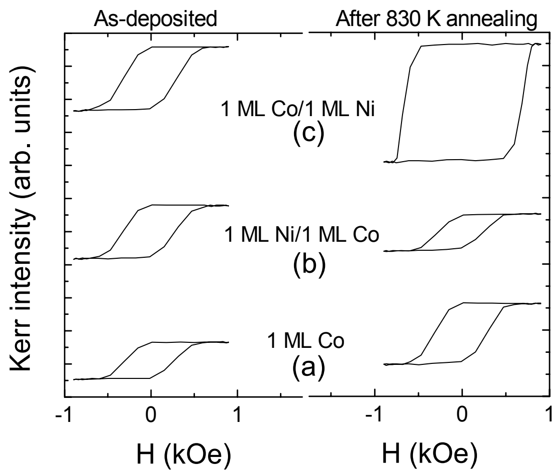

Fig. 3-33 Room-temperature hysteresis loops for the as-deposited samples and the samples after 830 K annealing for 20 minutes. (a) 1 ML Co/Pt(111), (b) 1 ML Ni/1 ML Co/Pt(111), and (c) 1 ML Co/1 ML Ni/Pt(111)

From the section 3-5-1 to 3-5-6, we show some fundamental properties for the Ni and Co layer on the Pt(111) surface. The corresponding T_C data are collecting in the Table 3-2.

TABLE 3-2 Curie temperature of the corresponding sample after 830 K annealing.

Sample	T_C (K)
1 ML Co/Pt(111)	490
1 ML Ni/1 ML Co/Pt(111)	325
1 ML Co/1 ML Ni/Pt(111)	530

Deposition or incorporation of Ni on Co attributed to a slight increase of the MO signal may lead to the reason as follows: The charge transfer at the interface from Co to Ni affects the exchange–split minority and majority bands therefore increases the Co spin moment and reduces the Ni spin moment. In the detail XMCD study by Dhesi et al.,[155] they found that the Co spin moment gives an increase from $1.4\mu_B$ to $1.9\mu_B$ after deposition 1 ML of Ni. This statement may match to our inference of surface mixing in our P-MOKE measurement of 400 to 480 K in the left of Fig. 3-33. The reports indicated the Ni moment reduced to $0.4\mu_B$ and $0.22\mu_B$ for the 2 and 0.2 ML of Ni films, respectively. Such charge redistribution as a function of film thickness of Ni reduces the Ni d^8 weight and increases the diffuse magnetism arising from delocalized *sp* states. These observations indicate that the electronic hybridization changes as a function of film thickness. The hybridization is proportional to the square root of the number of neighbor atoms.[156] When it reduces at the surface, the d^8 weight in the ground reduces. James *et al.* have once used the linear-muffin-tin-orbital with coherent-potential approximation method (LMTO-CPA) to calculate the magnetic moment of binary alloy, such as $Co_{1-x}Ni_x$, it is surprising that the moment of random alloy of fcc $Co_{75}Ni_{25}$ and $Co_{25}Ni_{75}$ has a little larger than that of the order alloy.[157] The possible structure may be obtained by mixing of Co and Ni layers such as the Co/Ni/Pt and Ni/Co/Pt cases.

On the other hand, before we discuss the different behavior as the intersecting layer of Ni into Co/Pt(111) system. Let us first look at the behavior of the $H_C(T)$ as given in Fig. 3-34 and 3-35. The diffusion occurring at the interfaces and column boundaries strongly contributes to the mechanism of H_C in the annealed samples.[158] The coercivity as a function of temperature for the sample of 1 ML Ni/1 ML Co/Pt(111) was given in Fig. 16. As we know, the relation between the coercivity and the temperature for ultrathin films or multilayers can be described as the following formula[159]

$$H_C = \frac{2K}{M_s}\left(1-\sqrt{\frac{25kT}{KV}}\right) = H_{C0}\left(1-\sqrt{\frac{T}{T_B}}\right) \quad (3\text{-}10)$$

where K is the magnetic anisotropy, M_s is the saturation magnetization at 0 K, V is the particle volume, k is the Boltzmann constant, H_{C0} is the coercivity at 0 K, and T_B is the blocking temperature. The coercivity is in general related both to the nucleation process and to the pinning of the domain wall motion. On the other hand, the H_C can be altered by interaction between the magnetic adsorbed atoms and substrate atoms. From the above relation, the volume of the magnetic particle in our layered system can be changed by interdiffusion. Different annealing temperature and different sample preparation have possibly created specific magnetic layered structure and reveal abnormal magnetic properties.

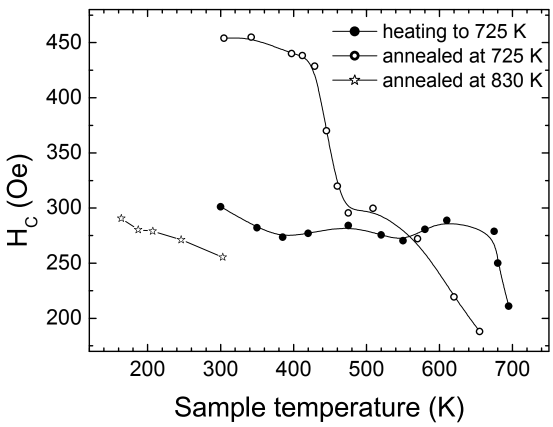

Fig. 3-34 The temperature dependence of coercivity for 1 ML Ni/1 ML Co/Pt(111): (a) Heating up to 725 K, (b) after annealing at 725 K, and (c) after annealing at 830 K. Other descriptions see in the text. The continuous lines are guides to the eye.

Fig. 3-34 shows the relation of the H_C as a function of temperature for the 1 ML Ni/1 ML Co/Pt(111) sample. The trend of the H_C follows the relation of $\theta_k - T$ given in Fig. 3-25. In the process of surface mixing of Ni and Co and the initial bulk diffusion for the Co, H_C has an increase of about 30 to 50 Oe. In the mixing or diffusing process, surface particles may be smaller than the flat layer because the temperature may promote the nucleation of the adatoms and increase the density of the nucleated particles.[160] Since the H_C is proportional to $V^{-1/2}$, the H_C increases when we neglect the magnetic anisotropy K and the saturated magnetization M_s which from the neglected increase of the MO signals. After the sample annealed at 725 K for 20 min, we found a different behavior of the H_C which is indicated in Fig. 3-34. The H_C drops rapidly from 430 Oe at 430 K to 300 Oe at 475 K. The interesting magnetic property will be discussed in the future study. Author believes this may be attributed to the slight change of the microstructure in the annealing range. Furthermore, in the final third anneal up to 830 K, the H_C value then return to about 300 Oe but at the low-temperature of 160 K.

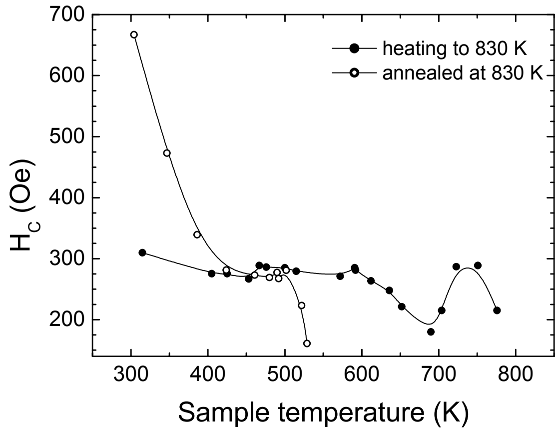

Fig. 3-35 The temperature dependence of coercivity for 1 ML Co/1 ML Ni/Pt(111): (a) Heating up to 830 K and (b) after annealing at 830 K. Other descriptions see in the text. The continuous lines are guides to the eye.

From the heating process of 1 ML Co/1 ML Ni/Pt(111) sample, the H_C–T relation given in Fig. 3-35 is very different from that of the mirror system of 1 ML Ni/1 ML Co/Pt(111) until the temperature is over 600 K. The H_C for the Ni/Co/Pt film over 600 K did not decrease too much as T > 675 K. Then it decreases as the T_a increases. For the Co/Ni/Pt film, the H_C just diminished slowly when T_a < 700 K. But we see a clear jump of the H_C increases from about 200 Oe at 700 K to 290 Oe at 725 K. Let us recall our AES studies for the two samples, we found the Ni 102 eV Auger signals of the Ni/Co/Pt sample descend after T_a= 650 K but for the Co/Ni/Pt sample this drop occurred after T_a= 580 K. Apparently the content of Ni in the surface region for Co/Ni/Pt may be smaller than the Ni/Co/Pt. The residual Ni content on the surface strongly affected the surface magnetic anisotropy. Interestingly, we carefully compared the $\theta_k - T$ curve between the two samples. The $\theta_k - T$ curve for the sample of 1 ML Ni/1 ML Co/Pt(111) after annealed at 725 K is very similar to that of the 1st heating process for the sample of 1 ML Co/1 ML Ni/Pt(111). Moreover, the depth-profile analysis of the annealed 1 ML Ni/1 ML Co/Pt(111) sample indicated that most of the Co atoms are located in the top layers, but the Ni atoms diffuse into deeper interface of the bulk. Meanwhile, the surface structure determined by LEED we observed a dramatic transition from order to disorder in 650 to 725 K. LEED spot profile analysis can be used for the identification of island density on the surface. The diffracted spots after 650 K annealing was sharper and brighter than the vague and diffused spots at 725 K. We believed that the particle volume V after annealed at 650 K is smaller than that of at 750 K. That's why the H_C values of Ni/Co/Pt film are larger than the values of Co/Ni/Pt film in this range. Similarly, the unusual ascending of the H_C can be treated as the same point of view in the modification of surface structure. This assumption just corresponds to the surface structure of Fig. 3-26b and Fig. 3-26c. The (1×1) spots become much more bright and sharp. These order-disorder transitions are very interesting in the surface morphology change.

In the final anneal up to 830 K, the H_C of the Co/Ni/Pt film is following the relation of Eq. 3-10. The most interesting is that the H_C becomes very large even 670 Oe at RT and as the temperature increases the H_C shift from the value of 670 Oe to almost 270 Oe at 500 K. According the Eq. 3-10 of the H_C for thin film, we can obtain the H_{C0} = 1.8 kOe at 0 K and the blocking temperature T_B is about 660 K by the best fitting. Thus, we can estimate the magnetic anisotropy K for 1 ML Co/1 ML Ni/Pt system after the 830 K annealing is 2.6×10^6 erg/cm^3. This value is higher than 1 ML Co/Pt(111).[161] That's the reason the Co/Ni/Pt layer possesses large perpendicular anisotropy.

3-5-8 UPS studies for 1 ML Ni/1 ML Co/Pt(111) and 1 ML Co/1 ML Ni/Pt(111)

UPS is a surface-sensitive technique used for observing the electronic valence band near Fermi energy. Fig. 3-36 shows the evolution of the UP spectra for the 1 ML Ni/1 ML Co/Pt(111) sample during annealing. Fig. 3-36a is the original electronic distribution of UP spectra. Because our UP system is designed for the integrated mode, the UP intensity can only be observing the mixing density of states near the surface. The photon energy of excited He I (21.2 eV=585 Å) is used for the light source. The bottom of the spectrum in Fig. 3-36a corresponds to the as-deposited sample of 1 ML Ni/1 ML Co/Pt(111) at RT. As the T_a increases, the *d*-band intensities were lower than as-deposited UP spectra. But the variation is not clear. So that the difference spectra which minus the spectrum at RT as the background would be expected for a better observation. In Fig. 3-36b the results indicated the variation begins after 600 K, we see the increase of the *d*-band intensity. The difference *d*-band intensities from Fermi edge to the binding energy of 4.2 eV gradually emerged in the range of 600 to 803 K. For the reason, we measured peak height of Fermi edge which is shown in Fig. 3-36c. The peak height did not change obviously until T_a=600 K. As for the increase of Fermi peak height, we believe the increase is coming from the Pt *d*-band states. Because the *d*-band structure for a clean Pt(111) substrate just extends from binding energy peak at 4.2 eV and a very sharp peak near the Fermi edge. From these strong evidences by the aforementioned surface analysis, thus we conclude that the segregation of Pt to the top surface is another possible mechanism for explaining the layer-alloyed with low-T_C.

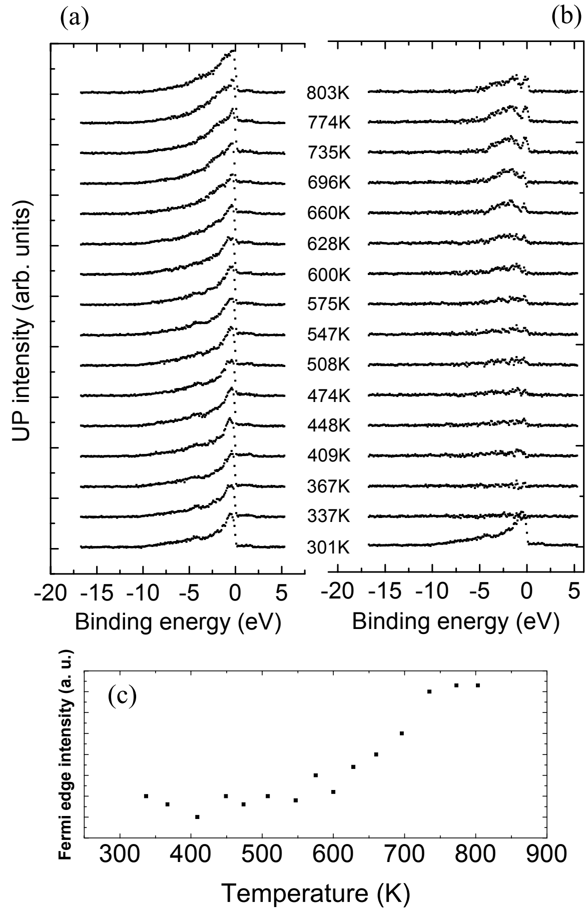

Fig. 3-36 The variations of the UP spectra for 1 ML Ni/1 ML Co/Pt(111) versus the annealing temperature from RT to 800 K. (a) original spectra, (b) difference spectra (c) the measurement of the height of the Fermi edge. The obvious increase after 575 K is corresponding to the increasing states of the Pt d-band.

The alteration of magnetic properties in a system is usually related to the change from electronic properties. Thus, the mirror system of 1 ML Co/1 ML Ni/Pt(111) sample were also studied by UPS for a better understanding of magnetic properties. The original spectra are given in Fig. 3-37a. As the same as the Ni/Co/Pt system, original spectra can not afford useful information for observing the evolution of electronic states. To a better review, we provided the difference spectra which compare with the spectrum at RT. Then we observed a clear modification near Fermi edge as given in Fig. 3-37b. The peaks near the Fermi edge have three significant increases in the range of 400 to 450 K, 500 to 575 K and 660 to 800 K. The Fermi edge intensities as a function of temperature were shown in Fig. 3-37c. Comparing with the AES and the P-MOKE studies of the system, the increase is an important index for understanding the change of the magnetic properties. In the compositional analysis by AES, ranges from 400 to 450 K and 500 to 575 K just correspond to the surface mixing states of Co–Ni and segregation of Pt to the top layer. In these two ranges, the $\theta_k - T$ curve just has a major peak at 450 K and a minor peak around 575 K. Finally, the peak near the Fermi edge emerged again higher than 660 K is attributed to the Pt-dominated states in the *d*-band. From the compositional analysis by AES, we can confirm the surface occupied by Pt atoms.

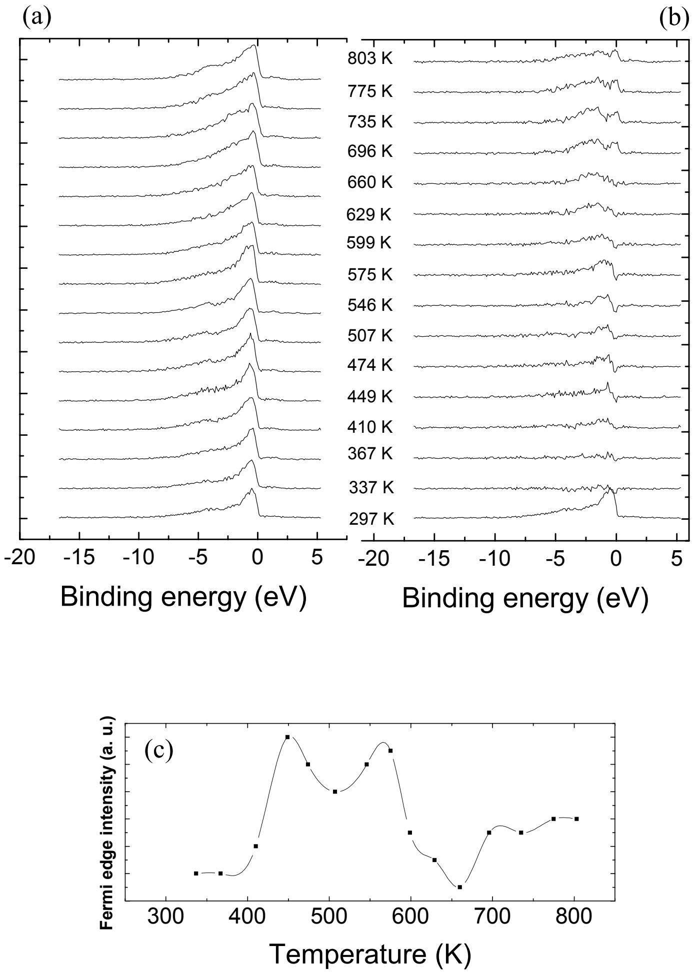

Fig. 3-37 The variations of the UP spectra for 1 ML Co/1 ML Ni/Pt(111) versus the annealing temperature from RT to 800 K. (a) original spectra, (b) difference spectra (c) the measurement of the height of the Fermi edge. The increase from 400 to 450 K and from 500 to 575 K is corresponding to surface mixing of Co and Ni and segregation of Pt states to the top layer. The Fermi edge height finally saturated due to the d-band of Pt dominated after 650 to 800 K. The surface finally forms a Pt-rich layer.

We know that electronic charge transfer from one atom to another or the change of the geometric structure may simultaneously alter the corresponding magnetic structure. Daalderop *et al.* using first-principles local-spin-density calculations showed that the Ni/Co interface anisotropy is controlled by *d*-state occupancy near Fermi level.[162] Dhesi et al. using x-ray magnetic circular dichroism (XMCD) once observed a film thickness of Ni on Co/Cu(001) below 2 ML the number of holes and the spin moment per hole show a gradual decrease, while the orbital moment per hole and the spin-orbital interaction show a gradual increase in magnitude.[163] Incorporation of Ni on Co/Pt(111), result in a redistribution of charge, which may increase the Ni *d*-state occupation and reduced the *d* occupancy of Co. To detect the electronic charge distribution near Fermi level, we used the UPS technique to observe the evolution of electronic *d*-band structure. The result indicated the saturated Kerr rotation in the Ni/Co/Pt and Co/Ni/Pt annealed films is larger than that of as-deposited layered structure. The bulk diffusion process made redistribution of charge density increasing the Co spin moment and reducing the Ni spin moment. Thus, the variation of the d-band peak near the Fermi edge in the UP spectra is a strong evidence for supporting this statement.

In this section, the structural and magnetic properties of 1 ML Ni/1 ML Co/Pt(111) was studied by means of AES, LEED, UPS and SMOKE. From the growing curve by AES and (00) spot intensity analysis by LEED the epitaxial of Ni on the 1 ML Co/Pt(111) follows 2 ML layer-by-layer growth mode. The alloying effect and surface mixing effect in the annealing are very interesting for the sample of 1 ML Ni/1 ML Co/Pt(111). Co and Ni are well-known mutual miscible solids and can form alloys with Pt. In our ultrathin film system, we first observed a mixing effect of Co and Ni in the temperature range of 400 to 480 K. Co and Ni atoms then diffuse simultaneously when the annealing temperature is higher than 600 K. In the depth profile analysis and the calculation of relative chemical compositions, strong evidence shows the diffusion volume of Ni is larger than that of Co. Co layer forms surface alloy about few layers but the Ni diffuses to the deeper layer.

The magnetic properties of 1 ML Ni/1 ML Co/Pt(111) were performed by P-MOKE. Kerr rotation as a function of temperature shows some unusual magneto-optical properties. We found a slight increase in the surface mixing of Ni and Co and alloying effect of Co–Pt contribute to a significant enhancement in the temperature of 575 to 620 K. When the sample is annealed at 725 K the Kerr rotation enhanced about two times than the as-deposited layered film. But we obtain near room-temperature T_C for the annealed sample when T_a is 830 K. Higher temperature annealing can create different surface concentrations of Co, Ni and Pt in the surface layers. Different surface compositions for the Co-Ni-Pt alloy layers may possess different magnetic properties. The low-T_C of Ni–Pt layers might be the leading character with the high-T_C Co–Pt layer in our annealed Ni/Co/Pt system. Thus, 1 ML

Ni deposited on the pre-annealed Co–Pt(111) layer in different T_a was also studied to find the role of Ni in the Co-Pt alloy layer. Interestingly, the T_C of the annealed sample is a function of T_a. When the T_a is higher than 500 K, the T_C is shift from 485 K to 275 K. The mean surface composition can estimate by relative Auger signals in the top at least 6 ML. The result indicates the Pt-rich surface and the Ni concentration on the top layers may cause the low-T_C layered film.

The MO properties of 1 ML Co/1 ML Ni/Pt(111) was also used to compare the 1 ML Ni/1 ML Co/Pt(111). The same annealing condition was used but a very different effect in the temperature range of 600 to 725 K. For Ni/Co/Pt layer, θ_k has a maximum value about 0.06º in this range but for Co/Ni/Pt layer has a minimum approach to 0. This unusual and interesting phenomenon may be attributed to the diffusion volume of Ni layers.

The Co/Ni/Pt annealed films can be provided with high coercivity, large Kerr rotation and high-T_C near room temperature. On the contrary, the Ni/Co/Pt annealed films with low coercivity, low Kerr rotation and low-T_C. Such artificial magnetic heterostructure in thin film system is worth to study and very promising for application use in the future.